Journal of Building Engineering 114 (2025) 114268

Contents lists available at ScienceDirect

Journal of Building Engineering

journal homepage: www.elsevier.com/locate/jobe

Experimental and numerical analysis of Tuned Sloshing Dampers and Liquid Column Vibration Absorbers for the vibration control of a multi storey frame using fluids of different viscosities

Andrea Vázquez-Greciano [a,b,*], Nicola Buratti [b], Antonio Aznar López [a], Jesús María Ortiz Herrera [a]

[a] Department of Building Structures and Physics, Universidad Politécnica de Madrid, P° Juan XXIII, 11, 28040, Madrid, Spain
[b] Department of Civil, Chemical, Environmental and Materials Engineering, Alma Mater Studiorum -Università di Bologna, Via Zamboni, 33, 40126, Bologna, Italy

ARTICLE INFO

Keywords:
Tuned Sloshing Damper (TSD)
Liquid Column Vibration Absorber (LCVA)
Shake table
Viscosity
Structural vibration control

ABSTRACT

Tuned Liquid Dampers (TLDs) dissipate energy through the out-of-phase fluid motion inside a container relative to a structure. This study experimentally and numerically analyses the two main TLD configurations: Tuned Sloshing Dampers (TSDs) and Liquid Column Vibration Absorbers (LCVAs).

Shake table tests are used to evaluate the Frequency Response Function of a four-story scaled frame with and without TSDs and LCVAs, comparing the effect of water and two commercially available non-organic fluids of diverse viscosities under different horizontal harmonic base excitation amplitudes.

A numerical analysis supports the interpretation of the influence of key parameters – mass, damping and frequency of the device – and evaluates the precision of existing formulations found in the literature and codes. For TSDs, the experimentally measured and numerically defined mass and frequency agree with the literature. For LCVAs the existing mass participation prediction does not align with the results: only 25 % of the total fluid mass, corresponding to the fluid inside the columns, is effective. Additionally, a new LCVA frequency formulation is proposed, reducing prediction error from 15 to 2 %. The amplitude and viscosity-dependence of the damping ratio lead to defining different optimal fluid selections depending on the container: high viscosity fluids improve surface control and vibration suppression for TSDs, reducing both the response at resonance (99.5 %) and the maximum response (84 %). For LCVAs, higher viscosity causes excess damping and non-optimum performance. In this case water yields the best resonance reduction (98 %). These findings are aimed at refining the practical application of TLDs and improving their numerical definition.

* Corresponding author. Department of Building Structures and Physics, Universidad Politécnica de Madrid, P° Juan XXIII, 11, 28040, Madrid, Spain.

E-mail addresses: andrea.vazquez.greciano@upm.es, andrea.vazquez3@unibo.it (A. Vázquez-Greciano), nicola.buratti@unibo.it (N. Buratti), antonio.aznar@upm.es (A. Aznar López), jesusmaria.ortiz@upm.es (J.M. Ortiz Herrera).

https://doi.org/10.1016/j.jobe.2025.114268
Received 30 July 2025; Received in revised form 19 September 2025; Accepted 30 September 2025
Available online 3 October 2025

1. Introduction

Structural control methods have been developed over the years to mitigate vibration in structures, they hold particular significance in the management of the response of structures to dynamic loads, which can be produced by everyday phenomena such as wind, traffic and even pedestrian loading but can also be due to extraordinary events such as earthquakes or explosions. In the first scenario, the aim of structural control lies in maintaining serviceability limits, regulating the possible discomfort caused to the users and reducing the risk of structural fatigue, while in the second one close attention is paid to ensuring safety within ultimate limits and preventing structural failure.

Dynamic Vibration Absorbers (DVAs) are mass-damper-spring systems that can be used to protect structures from inadequate vibration levels. The well-known Tuned Mass Dampers (TMDs), together with their fluid counterparts, Tuned Liquid Dampers (TLDs), fall into this passive structural control category. TLDs have attracted great interest since they were first applied in civil structures in the 1980s [1,2] since they rely entirely on the out-of-phase movement of a liquid, typically water, inside a container with no need of external mechanisms, thus resulting in low cost in installation and maintenance of these devices which can be temporarily or permanently applied in already existing structures. Further advantages result from their inherent characteristics: they are not limited to unidirectional vibration absorption, and they can be easily tuned just varying the fluid depth.

Based on the shape of the container, TLDs can be categorised into Tuned Sloshing Dampers (TSDs) and Tuned Liquid Column Dampers (TLCDs). TSDs are generally rectangular or cylindrical containers that rely on the sloshing motion of the liquid in the direction of the movement. TLCDs are U-shaped containers in which the fluid oscillates between interconnected columns. Generally, an orifice is located on the horizontal section to account for damping derived from the fluid passage. Over the years, a vast number of proposals have been made to passively improve the effectiveness of TLDs. These include variations in the containers' shape and arrangement. Liquid Column Vibration Absorbers (LCVAs) are a TLCD variation in which the cross-sectional area of the columns is different from that of the horizontal section, allowing for greater versatility and adaptability. Another form of enhancement is considering using fluids other than water. Although water is an accessible resource, it presents a low inherent density and damping. Using denser and more viscous fluids can improve the performance of TLDs while preserving their distinctive characteristics that make them particularly advantageous. Recent extensive reviews with emphasis on the different enhancement possibilities, configurations, numerical evaluation, materials used, and limitations can be found in Refs. [3,4]. Some of the most recent investigations experimentally evaluate different enhancement possibilities of all types of TLDs (TSDs [5], TLCDs [6] and LCVAs [7]) while establishing a mathematical definition for their characterisation.

The first numerical models used to describe the behaviour of TSDs use nonlinear shallow water wave theory, date back to the 1980–90s [8–13] and were validated for water as the sloshing fluid for free and harmonic oscillations for continuous free surface, which is the case in which breaking of waves does not occur. Although TSDs generally contain water, the use of other fluids has also been studied for SDOF structures for various viscosities up to 30 times more viscous than water [14], including non-Newtonian fluids [15] and custom-prepared magnetorheological fluids [16], and in MDOF systems with varying fluid density of a water-sugar solution [17] and viscosities ranging from a third to twice as water's viscosity and fluids less dense than water (acetone and propanol) and more dense than water (chloroform and mercury) [18], as well as with a density-variable sand-water mixture [19]. It was concluded that there is an amplitude-dependency of the response and that both viscosity and density can improve the controlled frame response up to certain values that, when exceeded, lead to poorer effectiveness of the DVA.

The first studies regarding TLCDs date of the late 1980s [20] and further parameter optimization approaches were developed in the next decade for SDOF [21–23] and MDOF models [24,25]. The development of LCVAs occurred concurrently and followed the bases presented in TLCD theory [23,26–29]. In these types of devices, close attention has been paid to numerically [30,31] and experimentally [32–34] studying how different parameters, such as the mass ratio of the damper to the structure, length ratio of the horizontal section with respect to the total fluid length, or orifice opening ratio of the area of the orifice to the area of the horizontal section, affect water-based TLCDs and LCVAs. The use of fluids different from water has been reported in SDOF structures for water-denatured alcohol solutions [27], water-glycol solutions and a passive configuration of magnetorheological fluid [35], with 1.4, 18 and 51 times the dynamic viscosity of water, respectively. The use of viscous lubricants has also been studied experimentally on a MDOF structure [36]. Fluids denser than water have been reported to lead to better performance [37] also in MDOF systems [38] due to an increment in the fluid mass for the same volume. It was concluded that viscosity has a direct impact in increasing the damping coefficient and in controlling the fluid motion, and that it is amplitude dependent. Therefore, excessively high viscosity values can suppress the fluid movement, thus resulting in poorer DVA performance. Generally, the denser the fluid, the smaller the displacement of the structure equipped with DVAs.

While the literature offers studies of TLDs that consider the aforementioned aspects separately, a lack of comprehensive investigations specifically examining the effectiveness of Tuned Sloshing together with Column Liquid Dampers in MDOF structures is detected. In this context, recent studies compare the performance of TSDs [39] and TLCDs [40] with that of TMDs. Two main conclusions can be derived from these studies: first, that TLDs exhibit a better performance if spatial stroke limitations exist, which is particularly relevant in buildings where loss of useable area is a concern; second, it is remarked that some of the key parameters that define TLDs such as mass and damping need to be optimised when water is used as the working fluid in order to fully improve their performance compared to their mass-based counterparts. Kebeli et al. [41] have recently carried out an experimental comparison of the performance of TSDs and TLCDs in a MDOF frame, highlighting the effect of different fluid heights. Earlier studies [42–44] examined the performance of each device separately, also considering their placement on different floors of the frame. In this regard, the exploration of alternative liquids beyond water, with non-degradable inorganic fluids for different amplitudes of motion remains at a shallow level of study.

To address this, the present study compares the response of a four-story scaled steel frame under varying horizontal harmonic excitations before and after the separate inclusion of the main TLD geometries adopted in practical engineering: TSDs and LCVAs, with and without orifices. The comparative study includes water as a benchmark and also identifies and explores the behaviour of two commercially available non-organic fluids. This comparative study facilitates the identification of the most suitable fluid depending on the selected geometry.

Parallelly, a numerical analysis is carried out to corroborate the experimental investigation and to evaluate the precision of the existing formulation found in the literature and codes used to model these devices, which has been found to have insufficient consensus in the bibliography, more evidently in LCVAs. In this regard, the numerical analysis considers three key parameters -effective mass, damping and natural frequency of the device- and a model updating process retrieves their optimised values in accordance with the experimentally observed behaviour. It evidences and addresses the inconsistencies detected in the literature, proposing new formulations for the definition of the effective mass and natural frequency for the LCVA studied, together with values of damping for all the fluids considered.

This analysis is crucial for the proper analysis, definition and characterisation of TSDs and LCVAs for their practical application to building and civil engineering.

In this paper, first, the TLD working principle is presented based on TMDs due to their similarities, followed by an overview of the existing formulation of TSDs and LCVAs, setting the stage for subsequent discussions. Next, the experimental setup is expounded. Firstly, the frame characteristics are described. Then, the studied fluids and TLDs characterisation are provided, in which the issues regarding the tuning are addressed. Then, an overview of the experimental campaign is presented. The experimental and numerical results are examined and discussed in subsequent sections. In the final section of this work, the conclusions derived from the experimental and numerical investigations are drawn.

2. TLD working principle

TLDs are passive control systems in which a fluid inside a recipient is used to dissipate energy through an out-of-phase movement with respect to the main structure. TLDs follow the same basic principles as Tuned Mass Dampers, which can be defined, in their simplest form, as systems comprising a mass, a dashpot and a spring. Because of their similarities, a brief formulation of TMDs and how each component affects the structural response is first presented, followed by a more precise TLD and LCVA formulation.

2.1. TMD formulation

TMDs were originally described by Frahm in the 1900s [45] as means to reduce the vibration of a SDOF structure through the attachment of a secondary mass. Their working principle relies on the idea that, when the primary mass or mass of the structure (m_s) experiences periodic vibrations near its natural frequency, resonance initiates increasing amplitudes of motion. These can be mitigated with the inclusion of a tuned secondary mass, the damper mass (m_d), into the system. The simplest mass absorber scheme considers zero damping and is depicted in Fig. 1. The equations of motion of the primary and secondary systems are defined in Equations (1) and (2) and their solution is expressed in Equations (3) and (4) respectively.

$$m_s\ddot{u}_s + k_s u_s + k_d(u_s - u_d) = F(t) = F_0 \sin(\omega t) \tag{1}$$

$$m_d\ddot{u}_d + k_d(u_d - u_s) = 0 \tag{2}$$

$$u_s(t) = A_1 \sin(\omega t) \tag{3}$$

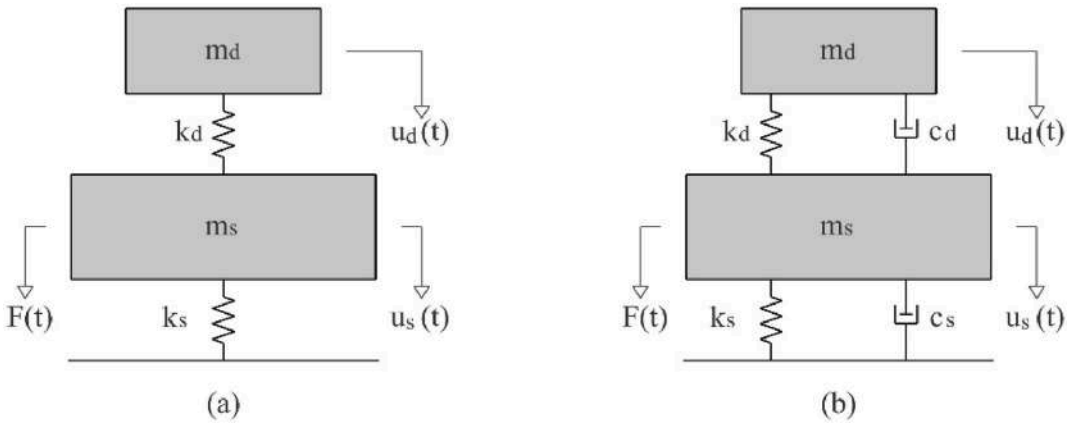

Fig. 1. Mass absorber scheme: (a) Frahm model, (b) Tuned Mass Damper.

$$u_d(t) = A_2 \sin(\omega t) \tag{4}$$

In the equations of motion, the subscripts s and d refer to the structure and the damper, respectively. Therefore, the mass of the structure is m_s, its stiffness is k_s and the variable u_s represents the displacement of the main system. Consequently, m_d, k_d and u_d are used to refer to the damper mass, stiffness and displacement respectively. The frequency of excitation is referred to as ω.

Through derivation and substitution, it is obtained that when the frequency of the applied force coincides with both the primary system and the secondary system natural frequencies ($\omega = \omega_s = \omega_d$), the values of A_1 and A_2 are $A_1 = 0$, $A_2 = -F_0/k_d$. Here arises the effectiveness of mass vibration absorbers: the response amplitude of the main system (A_1) becomes zero since the spring in the secondary system exerts a force $-F_0$ that counterbalances the external force on the primary system F(t).

Introducing damping, as illustrated in Fig. 1b, the equations of motion are Equations (5) and (6), where the structural (c_s) and TMD (c_d) damping are included. In this case the amplitude of vibration does not reach zero at resonance but is greatly reduced instead.

$$m_s\ddot{u}_s + c_s\dot{u}_s + c_d(\dot{u}_s - \dot{u}_d) + k_s u_s + k_d(u_s - u_d) = F(t) = F_0 \sin(\omega t) \tag{5}$$

$$m_d\ddot{u}_d + c_d(\dot{u}_d - \dot{u}_d) + k_d(u_d - u_s) = 0 \tag{6}$$

In order to gain a better understanding of TMDs, it is also interesting to briefly mention how the relations that exist between the structure and the TMD mass and natural frequency and the device's damping coefficient have different effect on the structure equipped with a TMD response. A selection of cases to exemplify these parameters is shown in Fig. 2.

The ratio of the TMD mass to the structure mass, named mass ratio ($\mu = m_d/m_s$), directly affects the frequency bandwidth within which the device is effective. Larger mass ratios increase the frequencies at which the response is controlled, spacing out the lower peaks, shifting them away from the primary structure's natural frequency and reducing their response value. Typically, the mass ratio adopted in applications is in the order of μ = 1–5 % [46,47].

The damping ratio of the TMD, $\xi = c_d/(2m_d\omega_d)$, controls the amplitude of the response around two invariant points. Larger damping tends to reduce the structural response. However, over a certain value the response is transformed into a single-peak curve, meaning that implementing high damping coefficients is a counter-productive measure. The typical damping ratio of TMDs is approximately ξ = 3.5 % [48,49].

Lastly, the tuning ratio relates the frequency of the TMD to the natural frequency of the primary structure, $\beta = \omega_d/\omega_s$. A mistuning increases the maximum response of the SDOF at either the first or second frequency of the system. For this reason, a proper calibration of the absorber is crucial.

2.2. TSD formulation

TSDs are based on the same working principle of TMDs but exploit the movement of a liquid in place of a secondary mass. The general dimensions of rectangular TSDs, considered in this paper, can be seen in Fig. 3, which defines the length of the recipient in the movement direction (L), width (W) and height (H), fluid depth (h) and wave surface elevation (η).

Similarly to TMDs, Tuned Sloshing Dampers can be modelled as mass-dashpot-spring systems. The advantage of TSDs is that the

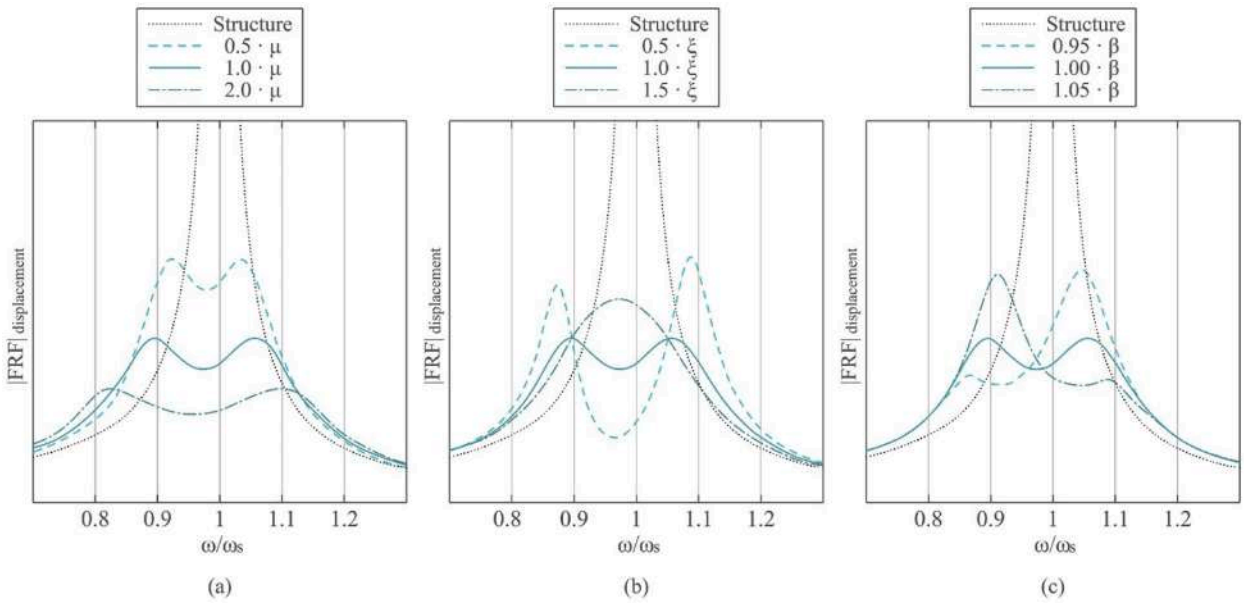

Fig. 2. Effect on the system response of: (a) mass ratio, (b), damping ratio, (c) tuning ratio.

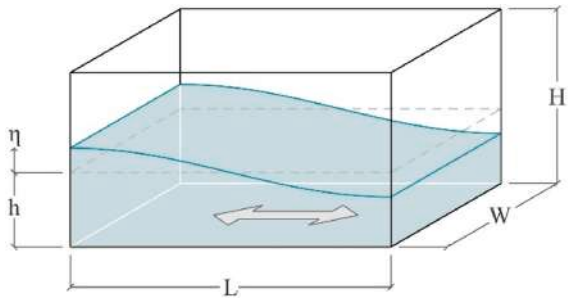

Fig. 3. Rectangular Tuned Sloshing Damper dimensions.

fluid that moves out of phase with respect to the main structure provides by itself with secondary mass, damping and stiffness without requiring any other external attachments.

The hydrodynamic fluid pressures that arise under horizontal excitations of the TSD can be used to explain the total fluid mass (m_{TOT}) division into impulsive or non-effective mass (m_0), in which the pressure is related to inertial forces on the walls, and convective or effective masses (m_n) associated with the sloshing in the different modes of vibration [50–53]. It is important to note that the convective fluid mass that participates in higher modes of vibration is very small compared to the mass associated with the 1st mode (m_1). Generally, the impulsive mass and the convective mass of the 1st mode represent over 95 % of the total fluid mass [51,54]. In this study, only the effective mass of mode 1 is considered.

Fig. 4 illustrates the models developed by Housner [50,55] and Yu et al. [56] from 1950s to 1990s to characterize TSDs, and a more recent combination of both of them [57], taken as reference in the present study since it allows us to consider both the division of the fluid into impulsive and first convective mass and the stiffness and damping associated with said effective mass. The impulsive mass is rigidly connected to the walls since it is considered to move together with the container. The convective mass represents the portion that participates in the out-of-phase sloshing movement and includes the spring and damper parameters.

One of the key parameters used to effectively apply TSDs is their frequency of sloshing (f_{TSD}), that depends solely on their geometrical configuration. It derives from linear wave theory [11,58] and it is defined in Equation (7) for the nth mode of vibration.

$$f_{TSD,n} = \frac{1}{2\pi}\sqrt{\frac{g}{L}\alpha_n \tanh\left(\frac{h}{L}\alpha_n\right)} = \frac{\omega_{TSD,n}}{2\pi} \tag{7}$$

The variable α_n is set for the different modes (n) as $\alpha_n = \pi\cdot(2n\text{-}1)$, and g represents the gravitational acceleration.

For rectangular TSD tanks, m_0 and m_1 can be defined with respect to the total fluid mass according to Equations (8) and (9) [50–53].

$$m_0 = \frac{1}{0.85}\frac{h}{L}\tanh\left(0.85\frac{L}{h}\right) m_{TOT} \tag{8}$$

$$m_1 = 0.26\,\frac{L}{h}\tanh\left(3.2\frac{h}{L}\right) m_{TOT} \tag{9}$$

The spring has a stiffness (k_1) that is described in Equation (10) [51].

$$k_1 = m_1\omega_{TSD,1} \tag{10}$$

The damping coefficient (c_1) can be calculated according to Equation (11) [11,59,60]. It is influenced by the wave surface elevation (η), fluid depth (h), container width (W), first convective mass (m_1), kinematic viscosity of the fluid (ν), angular frequency ($\omega_{TSD,1}$) and surface contamination factor (S) that takes a unity value for a fully contaminated surface [11,55]. The damping can also be expressed

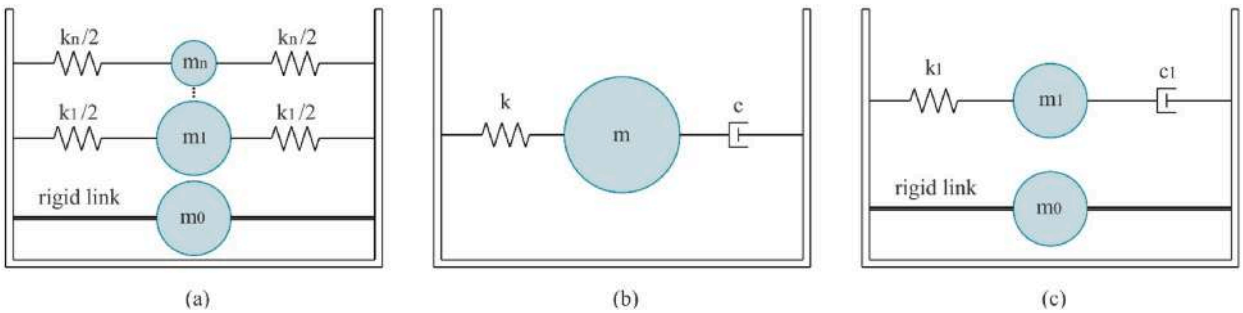

Fig. 4. TSD models: (a) Housner, (b) Yu et al., (c) Combined model.

in terms of the damping ratio (ξ) since $\xi = c_1/2m_1\omega_1$. Eurocode 8 [61] suggests taking $\xi = 0.5$ % for water and other fluids.

$$c_1 = \frac{m_1}{(h+\eta)\sqrt{2}}\sqrt{\nu\omega_{TSD,1}}\left(1+\frac{2h}{W}+S\right) \tag{11}$$

Therefore, Equations (5) and (6) can be reformulated as Equations (12) and (13):

$$(m_s+m_0)\,\ddot{u}_s + c_s\dot{u}_s + c_1(\dot{u}_s-\dot{u}_d) + k_s u_s + k_1(u_s-u_d) = F(t) = F_0\sin(\omega t) \tag{12}$$

$$m_1\ddot{u}_d + c_1(\dot{u}_d-\dot{u}_d) + k_1(u_d-u_s) = 0 \tag{13}$$

2.3. LCVA formulation

The global dimensions of LCVAs are annotated in Fig. 5. The cross-sectional area of the vertical and horizontal parts is defined by A_V and A_H respectively and can be obtained from the tank width (W) and column length (a) and horizontal height (b). The area ratio (r) is set as $r = A_V/A_H$. The length of the horizontal section between the columns is represented by L_H, and L_V is used to determine the vertical column height. Finally, the fluid displacement inside the columns is represented by u.

The frequency of the LCVA, as expressed in Equation (14), is essential to effectively apply these devices and can be derived from the frequency of their predecessors, the TLDs [62]. It depends only on the gravitational acceleration (g) and the effective length (L_{eff}) of the device.

$$f_{LCVA} = \frac{1}{2\pi}\sqrt{\frac{2g}{L_{eff}}} = \frac{\omega_{LCVA}}{2\pi} \tag{14}$$

It must be noted that there is no common consensus on the definition of L_{eff} and various approaches are found in the literature, as depicted in Fig. 6. Hitchcock et al. [26,27] were the first authors to study LCVAs and proposed their numerical formulation and studied how different geometrical combinations of uniform fluid flow in the vertical and horizontal sections, supported by experimental measurements, have an influence on the results. Their definition for L_{eff} is found in Equation (15). Shortly after, Chang and Hsu [28] compared different LCVAs designs and proposed a slightly different formulation that has been widely used [31–34] which involves how L_H and L_V are measured. They considered this modification to be insignificant if the size of transition zones between the vertical and horizontal parts is small. They did refer to the fact that turbulences and vortices generated near the transition regions and a non-homogeneous velocity of the fluid might affect the actual fluid motion. Following these considerations, Chaiviriyawong et al. [63,64] proposed an elliptical flow path numerical method that considers a variation in the fluid velocity in the transition zones and referred to an improvement in the model accuracy sustained by experimental tests on a shake table. Their definition of L_{eff} can be found in Equation (16).

$$L_{eff} = \frac{A_V}{A_H}L_H + 2L_V \tag{15}$$

$$L_{eff} = \frac{A_V}{A_H}L_H + 2L_V + \frac{\pi a}{2} \tag{16}$$

A mass-dashpot-spring system can be used to model LCVAs. The total mass of the fluid is expressed in Equation (17). The fluid density is denoted by ρ.

$$m_{TOT} = 2\rho W(aL_V + bL_H/2 + ab) \tag{17}$$

Different effective mass (m_{eff}) definitions are found in the literature. Some authors propose that the mass that participates in the movement equals the total mass [23,65], although other investigations suggest that only a fraction of the mass participates: the m_{eff} is sometimes considered to equal the mass inside the columns [24,34] while it is also referred to as the mass of fluid in the horizontal section that plays an important role since it generates the inertia force to control the vibration of the main structure [30,31].

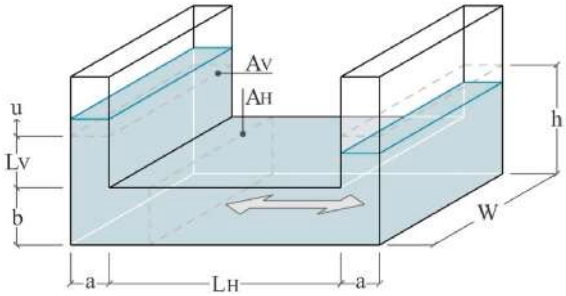

Fig. 5. Liquid Column Vibration Absorber dimensions.

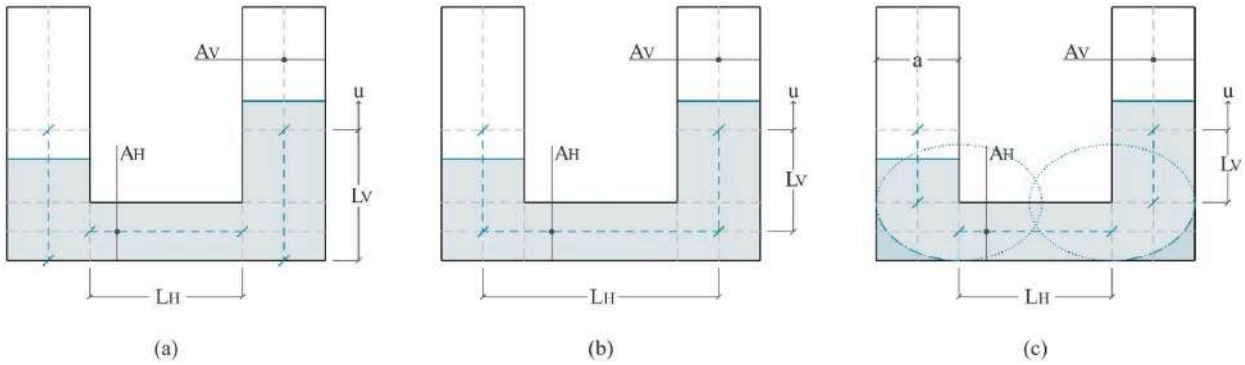

Fig. 6. LCVA approaches to define Leff: (a) Hitchcock et al., (b) Chang and Hsu, (c) Chaiviriyawong et al.

The stiffness definition can be derived from the consideration of a unit change in the fluid level and computing the restoring force produced by gravity, as seen in Equation (18) [30].

$$k_{LCVA} = m_{eff}\,\omega_{LCVA}^2 = 2\rho A_V g \tag{18}$$

The equivalent damping of LCVAs is defined by Chang and Hsu [28] as follows (Equation (19)), where σ_V refers to the standard deviation of the vertical fluid velocity and δ is the head loss coefficient, that occurs due to the cross-sectional area changes between the vertical and horizontal portions. The authors refer to δ as being determined experimentally for a specific LCVA geometry.

$$c_{LCVA} = \sqrt{\frac{2}{\pi}}\rho A_V r \delta \sigma_V \tag{19}$$

TMD Equations (5) and (6) can be rewritten as Equations (20) and (21) for LCVAs:

$$\left(m_s + m_{TOT} - m_{eff}\right)\ddot{u}_s + c_s\dot{u}_s + c_{LCVA}(\dot{u}_s - \dot{u}_d) + k_s u_s + k_{LCVA}(u_s - u_d) = F(t) = F_0 \sin(\omega t) \tag{20}$$

$$m_{eff}\ddot{u}_d + c_{LCVA}(\dot{u}_d - \dot{u}_d) + k_{LCVA}(u_d - u_s) = 0 \tag{21}$$

3. Experimental investigation

Dynamic experiments are conducted on a four-storey small scale steel frame mounted on a horizontally vibrating shake table. The vibration control of the structure is achieved through TSDs and LCVAs, and the use of different fluids under various base-amplitude conditions is studied for each type of container.

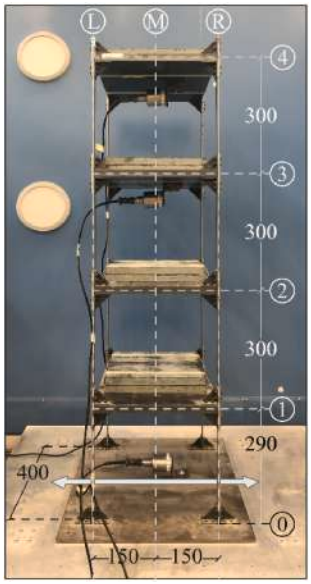

Fig. 7. Frame: main axes and dimensions (mm).

The shake table employed is self-built, has a size of 1.0 m × 1.0 m and is moved by an electromagnetic actuator from LinMot with a maximum horizontal payload of 1.0 kN, controlled with a PID algorithm by the LinMot Talk software. It imposes a unidirectional horizontal movement at the base of the frame. The excitation applied is harmonic and it can be controlled in terms of an amplitude scale for the displacement of the shake table and a time scale related to the frequency. The response of the frame is measured in terms of acceleration.

For acceleration data recording, Dytran Instruments series 3191 piezoelectric single axis accelerometers with a 10 V/g sensitivity are used. They can be applied for frequencies ranging from 0.08 Hz to 1,000 Hz, so they are suitable for the low frequencies studied. All the acceleration recordings are sampled at 200 Hz. The data acquisition platform used is CompactDAQ from National Instruments. The modules that measure the signal from the accelerometers are NI 9232, mounted on a cDAQ-9185 chassis. The NI 9232 modules are suitable for frequencies not lower than 1.0 Hz.

In the following sections, the properties of the frame are described, alongside with its experimental and numerical definition. Subsequently, the design of the TLDs is detailed through the fluids employed and the TSDs and LCVAs characteristics. Finally, an overview of the experimental campaign is presented.

3.1. Frame characteristics

For the experimental study, a four-storey small scale steel frame is used, as shown in Fig. 7. It has a constant storey-height of 300 mm, and it is 300 mm long and 400 mm wide (centre-to-centre). Floors are solid plates with dimensions 297 mm × 430 mm x 20 mm, and the columns are 3 mm × 30 mm rectangular sections, fixed to the upper and lower floors by 40 mm × 40 mm angle profiles. The mass of each floor can be adjusted with the incorporation of perforated 260 mm × 260 mm x 20 mm square steel plates that weight 10 kg each.

The mass of the frame itself is 78.8 kg, and a total mass of 158.8 kg was achieved through the addition of two 10 kg-square steel plates on each floor, required in order to lower the structural natural frequency to a range in which the TLDs can be tuned with a reasonable size. This is common practice, as described in the experiments run by Zahrai et al. and Xie et al. [66,67]. Although the frequency reduction could have also been achieved with a non-uniform distribution of the additional masses, a constant disposition in all floors was selected to better represent a building structure, in which the weight difference between floors is generally not substantial.

The symmetric frame is mounted on the shake table so that the unidirectional horizontal movement is applied in the direction of the frame's weaker inertia axis, as shown by Fig. 7. This setup can effectively retrieve information on the longitudinal modes of vibration of the frame, considering the longitudinal nature of the dissipative devices studied in this work.

The positioning of the accelerometers on the frame for the dynamic tests can also be seen in Fig. 7. A total of three accelerometers were mounted on the frame located in the centre of each floor along the direction of movement, because no torsional response is expected given the symmetric layout of the frame. Depending on the analysis performed, the accelerometers are placed at different heights. For the modal identification of the frame, the accelerometers were located on the 4^{th}, 3^{rd} and 2^{nd} floors so that broader information could be gathered from different floors considering the base as fixed. When the dynamic tests evaluate the response of different floors with respect to the input accelerations at the base, the accelerometers are distributed as follows: one on the top floor, one on the third floor and the last one at the base, in contact with the shake table so that the actual input accelerations could also be measured. This distribution enables the collection of the most significant data associated with the first mode of vibration.

3.1.1. Modal identification of the frame

The modal characteristics of the frame are obtained experimentally through free and ambient vibration testing. The results in terms of frequency are compiled in Table 1. Modal shapes were not identified from free vibration tests.

Free-vibration tests were carried out to retrieve the natural frequencies of the frame. In this case accelerometers were placed on the 4^{th}, 3^{rd} and 2^{nd} storeys; an initial displacement was imposed on the fourth storey which was then released to induce free vibrations. The signal recorded by the accelerometers is processed with Fast Fourier Transform (FFT) analysis, which transforms the time-domain information into the frequency-domain, thus obtaining the natural frequencies of the system from the peaks.

In addition to the free vibration tests, another methodology is employed to compare the frequency results and to extract the mode shapes; ambient vibration testing is used to identify the dynamic characteristics of the structure under ambient forces. To this purpose, a total of three accelerometers were placed on the 4^{th}, 3^{rd} and 2^{nd} storeys. The class of modal identification methods based on the measurement of structural response to ambient vibration falls within the discipline of Operational Modal Analysis (OMA), the ambient vibrations being random and unknown. Although OMA is typically applied in different contexts — such as in-service monitoring of civil or mechanical systems — it was adopted in this study due to the availability of previously developed and validated algorithms by

Table 1
Frequencies obtained from experimental ambient and free vibration testing and average result.

.Mode No.	Ambient vibration frequency (Hz)	Free vibration frequency (Hz)	Mean frequency (Hz)
Mode 1	2.012	2.018	2.015
Mode 2	6.046	6.032	6.039
Mode 3	9.450	9.443	9.447
Mode 4	11.480	11.558	11.519

the research group. These algorithms, implemented during earlier research activities [68], allowed for efficient data processing and modal identification without the need for additional development efforts. OMA relies on studying how a structure responds dynamically to external forces that cannot be controlled or measured, such as wind, traffic, microtremors, and so on. With these methods, therefore, by measuring only the output, and making assumptions about the input to which the system is subjected, it is possible to derive modal characteristics. Assuming that a structure is excited by white noise, meaning the input spectrum remains consistent, all its modes receive equal excitation. Consequently, the resulting output spectrum provides comprehensive details about the structure's characteristics. The previously mentioned forcings are rarely assimilated to white noise, so when observing the response of the structure, both input properties and modal parameters of the structure will be present. Despite this, it is possible to discern the structural modes from the excitation properties as the structural system possesses a narrowband response while the excitation system possesses a broadband response.

The technique used to extract modal parameters from the signals acquired by the frame is the Stochastic Subspace Identification method (SSI), which operates in the time domain [69]. Fig. 8 shows the results of the analysis carried out on 30 min of signal acquired at a sampling frequency of 200 Hz. It is possible to observe the stabilization diagram obtained by SSI analysis superimposed on the Power Spectral Density (PSD) of the signal acquired by the accelerometer placed on the 4th storey (accelerometer A1). The clustering algorithm proposed by Romanazzi et al. [68] was used in order to extract significant modal features, in particular the modal frequencies and shapes reported in Tables 1 and 2, respectively. The output of the clustering algorithm is illustrated in Fig. 9, where coloured circles indicate the stable poles of the stability diagram corresponding to the four modes of vibration identified. It is noted that the frequencies obtained by the two methods adopted are very consistent.

The mode shapes obtained from the ambient vibration data are summarized in Table 2.

3.2. Design of the TLDs

The characteristics of the fluids used in this study are described in the next section, followed by the presentation of the characteristics and design procedure of both the TSD and LCVA.

3.2.1. Fluid characteristics

Three different commercially available non-organic fluids with diverse viscosities and densities were used in the experimental campaign. The fluids are shown in Fig. 10.

The first fluid is water (hereinafter referred to as W), which allows for comparison of the response with other fluids. In this campaign, it has been dyed with black ink for better visualization. The second fluid (D in the following) selected is a water solution with modified acrylic polymers. Its density is 1.09 g/cm^3 and it has a dynamic viscosity of 50.00 cP. The third fluid (referred to as M) is a mixture of oils with a density of 0.87 g/cm^3 and a dynamic viscosity of 9.50 cP. A summary of the fluid characteristics can be found in Table 3. Both the dynamic (μ) and kinematic (ν) viscosities are listed.

3.2.2. TSDs characteristics

TSDs are rectangular-prism rigid containers. They are made of transparent plexiglass which allows seeing through to facilitate the visualization and evaluation of the fluid displacement. The dimensions of the TSD selected in this work have been optimised to procure the highest active mass (Eqn. (9)), considering that m_1 represented over 60 % of m_{TOT}, while at the same time refining the tuning of sloshing frequency (Eqn. (7)) to the first mode frequency of the structure. In this sense, the precision of the dimensions that define the frequency, that is, the container length (L) and the fluid height (h) was set to the millimetre. At the same time, maximum length

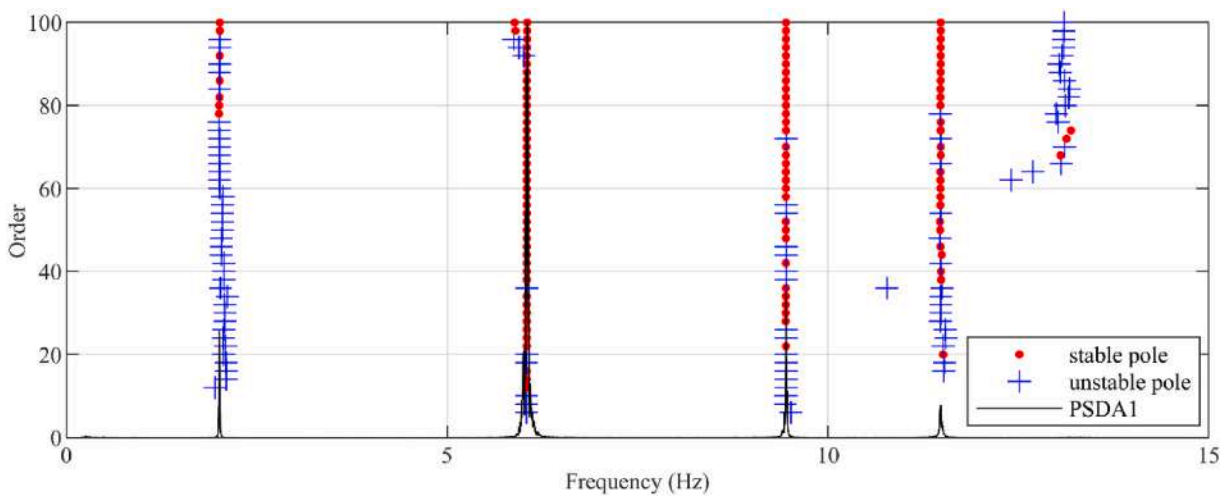

Fig. 8. Stabilization diagram obtained as a result of SSI analysis superimposed on PSD curve.

Table 2
Mode shapes derived from ambient vibration testing normalized for absolute maximum value = 1.

	Φ Mode 1	Φ Mode 2	Φ Mode 3	Φ Mode 4
Floor 4	1.00	−0.97	−0.83	−0.39
Floor 3	0.88	−0.06	1.00	1.00
Floor 2	0.63	1.00	0.57	−0.97
Floor 1	ND	ND	ND	ND

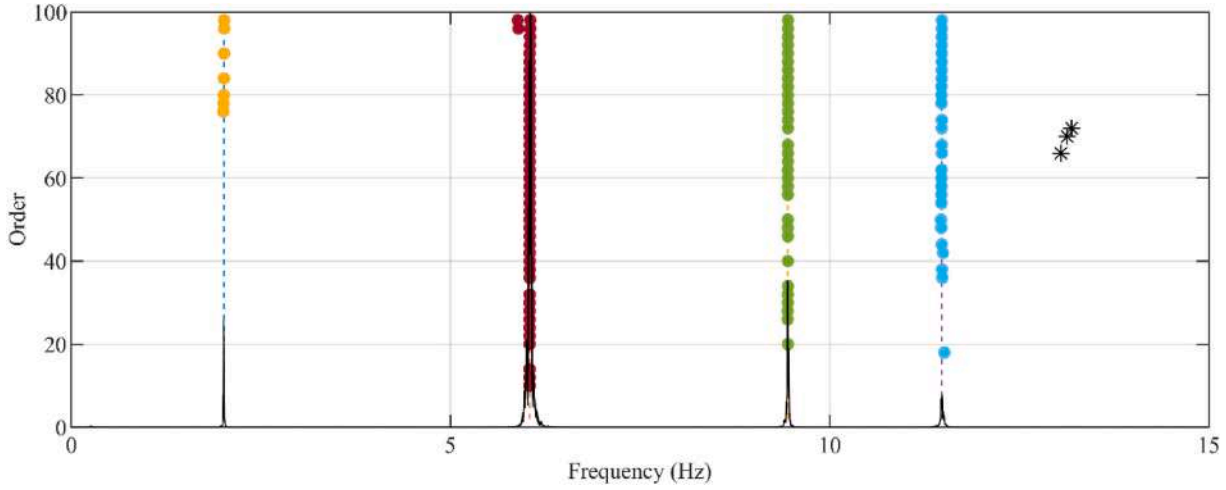

Fig. 9. Clustering of the stabilization diagram superimposed on the PSD curve.

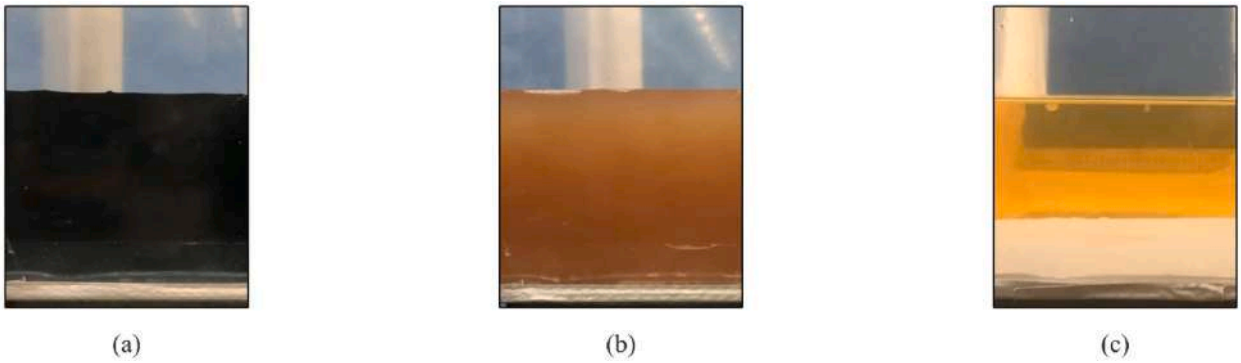

Fig. 10. Fluids: (a) W, (b) D, (c) M.

Table 3
Fluid characteristics: name, density, dynamic viscosity and kinematic viscosity.

Fluid	Density (kg/m^3)	μ (cP)	ν (cSt)
W	1.00	1.00	1.00
D	1.09	50.00	45.87
M	0.87	9.50	10.92

restrictions have been applied to ensure that one or several containers could be fitted inside the frame.

The selected TSD design is 144 mm long (L) and 430 mm wide (W) and the fluid depth (h) is 45 mm, as depicted in Fig. 11. This geometry allows the simultaneous installation of two containers per floor. The mass of each container is 1.10 kg. If fluid W is employed, the total fluid mass (m_{TOT}) per container is 2.79 kg and the impulsive (m_0) and convective (m_1) masses result in 1.02 kg and 1.77 kg respectively (see Section 2.2). If fluid D is selected, m_{TOT} is 3.04 kg, m_0 is 1.11 kg and m_1 is 1.92 kg. When fluid M is used, the total, impulsive and convective masses are 2.42 kg, 0.88 kg and 1.54 kg respectively. The mass ratio (μ) achieved is in the order of $\mu = 2.50$

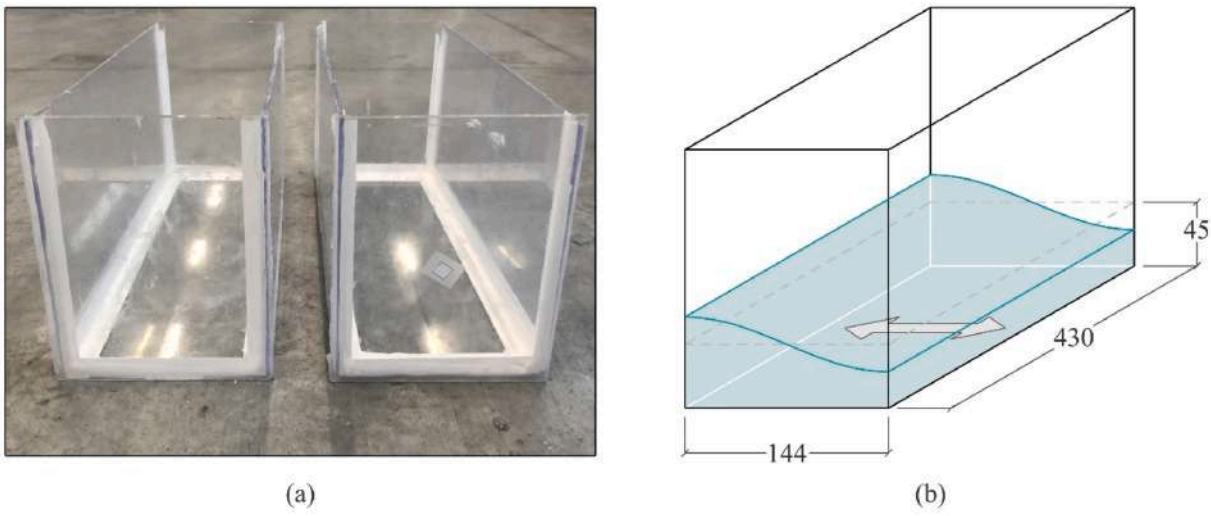

Fig. 11. TSDs used in the experimental tests, general dimensions.

%, and has been calculated as the effective mass of the device to the effective modal mass of the frame of the first mode (M_1^*), which has been calculated based on the FEM model described in section 5.1 (for reference, see Table 14). The mass ratio of two TSDs used simultaneously and tuned to the first natural frequency of the frame are 2.48 % for fluid W, 2.69 % for fluid D and 2.16 % for fluid M. Table 4 summarizes this data.

The frequency of the TSD was measured experimentally in order to validate the prediction given by Equation (7). To this purpose an impulse load is applied to initiate free vibration and its decay. The free surface movement is video recorded, and the maximum displacement is plotted against time using the open-source video analysis Tracker [70] and then analysed using FFT as means to obtain the frequency of sloshing. Table 5 displays the sloshing numerical, experimental and target frequencies. It shows that the frequency derived from Equation (7) and the frequency obtained from experiments differ by 0.45 %, which could be attributed to errors in the accuracy in the filling of the container with a margin of a reasonable range of ±0.5 mm, which directly affects the parameter of fluid height.

3.2.3. LCVAs characteristics

LCVAs are U-shaped transparent plexiglass containers. Three ribs that divide the container into four sections are included for support as seen in Fig. 12. Small holes are drilled near the bottom of each rib to ensure the fluid in all parts moves in unison by keeping the liquid height the same for all sections [71].

The geometry of the LCVAs is defined starting from the required effective length to achieve the target frequency, as defined previously in Section 2.3. Once L_{eff} is set as 124 mm, different area ratios, horizontal and vertical lengths are evaluated, according to the formulation described in the literature. The length ratio, defined as the relation of the horizontal length to the effective length, is kept around 0.6–0.7 [31,32,34,65], and the vertical length ensures the fluid always remains within the columns and does not reach the horizontal section [30]. Another requirement was to keep the area ratio smaller than unity, so that more volume of fluid could be obtained for the same L_{eff}. The initial dimensions follow the formulation suggested by Chang and Hsu [28] which has been adopted multiple times in the literature.

The LCVA container design is depicted in Fig. 12 and has a horizontal length of $L_H = 61$ mm, a width of $W = 461$ mm, the column sections are $a = 20$ mm and the horizontal ones are $b = 30$ mm, making the area ratio 2/3. The selected geometry allows for the simultaneous placement of two LCVAs on each floor.

For the initially selected design, the vertical column height was $L_{Vi} = 20$ mm. Therefore, the total volume of each container is 1765.63 cm^3, which implies that the total mass for fluid W in one container is 1.77 kg, for fluid D it is 1.92 kg, and for fluid M it is 1.54 kg. The mass of each container is 1.10 kg. The width of the container was set so that the total LCVA fluid mass was equal to the effective TSD mass for comparison purposes.

Table 4
Fluid characteristics: total mass, impulsive mass and convective mass (per container) and mass ratio if two tanks are used.

Fluid	1 container			2 containers
	m_{TOT} (kg)	m_0 (kg)	m_1 (kg)	$\mu = m_1 / M_1^*$
W	2.79	1.02	1.77	2.48 %
D	3.04	1.11	1.92	2.69 %
M	2.42	0.88	1.54	2.16 %

Table 5
Numerical, experimental and target TSD frequencies.

Frequency from Eqn. (7) (Hz)	Experimental frequency (Hz)	Target frequency (Hz)
2.021	2.012	2.015

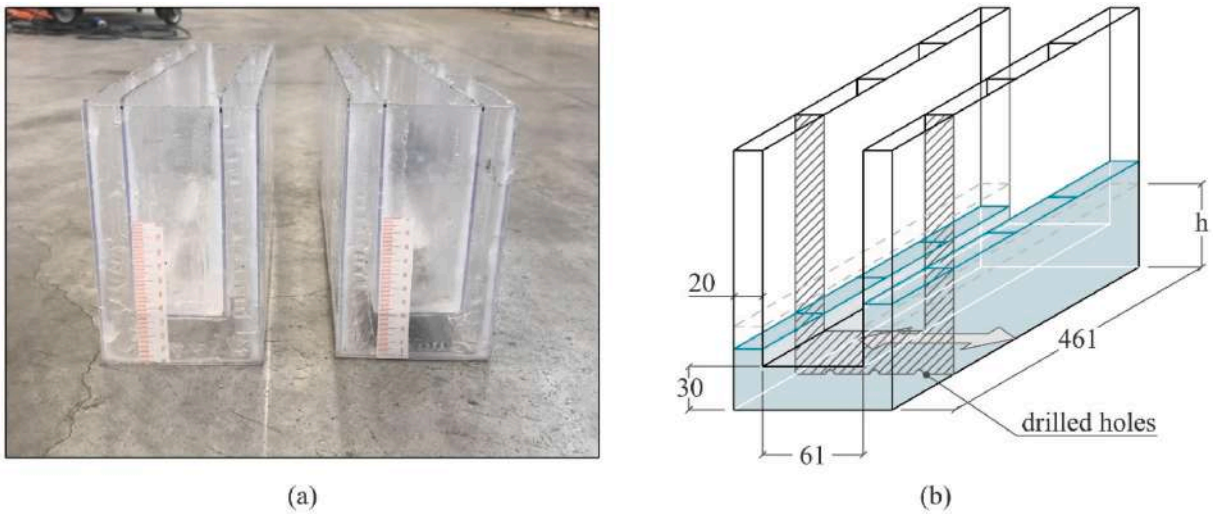

Fig. 12. LCVAs used in the experimental tests, general dimensions.

Again, the experimental validation of the frequency is done for comparison with the theoretical one obtained from Equation (14). An impulse load is applied to initiate free vibration and its decay, and the free surface movement is video recorded and the maximum displacement is plotted against time using the open-source video analysis Tracker as means to obtain the frequency of the device. It was observed that the experimental frequency was 16 % higher than expected, at around 2.25 Hz. Since a larger effective length gives a lower frequency, the LCVA container was filled up systematically until the target frequency was reached. The final selection results in an increment of the vertical length of 14 mm, resulting in $L_{Vf} = 34$ mm. Therefore, for the given geometry, the volume that gives the target frequency is 2021.79 cm^3. This increases the total fluid mass of a single container to 2.02 kg for fluid W, 2.21 kg for fluid D and 1.76 kg for fluid M.

For the purpose of better estimating the frequency, a variation of the definition proposed by Chaiviriyawong et al. [63,64] is presented in this work. In fact, it is observed that more accurate results are obtained if the Kinetic Energy in the transition zones takes the velocity profile as half of the one considered by Chaiviriyawong et al. The proposed L_{eff} described by the authors, presented in Equation (22), shows good agreement with the experimental results carried out in this campaign, where a is the semilength of the column, as seen in Fig. 13, which illustrates the dimension definition.

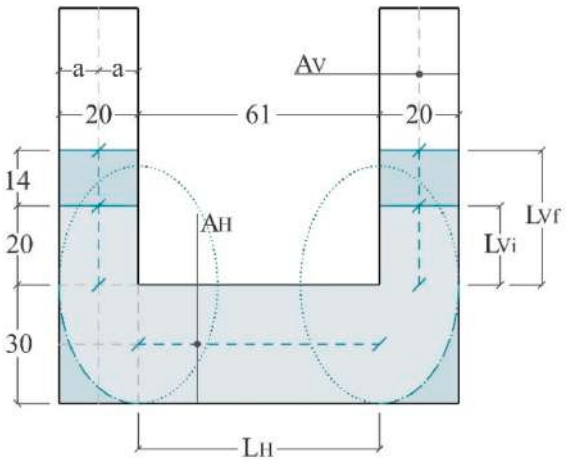

Fig. 13. LCVA used in the experimental tests, specific dimensions.

$$L_{eff} = \frac{A_V}{A_H} L_H + 2 L_V + \frac{\pi a}{2} \quad (22)$$

The frequencies obtained through the different numerical approaches are summarized in Table 6 and compared to the experimental and target values, for both the initial and final LCVA dimensions.

The addition of a plate with orifices in the middle section of the LCVA is also studied. These orifices are used to modify the head loss coefficient, and thus the damping. Different authors suggest opting for large blocking ratios to obtain bigger damping coefficient values, from 50 % up to a maximum of 80 % since a blocking area that is too large impairs the functioning of the device [22,33,34]. In this case, the container includes two ribs for support and two interchangeable blocking plates are employed. Holes of 15 mm in diameter are drilled in the plates. Two configurations are considered, a blocking ratio of 67 % is obtained with a total of 7 orifices, and a blocking ratio of 72 % is achieved with 6 holes. These configurations can be seen in Fig. 14.

3.3. Overview of the experimental campaign

In the present study, the MDOF steel frame with and without TLDs is studied under harmonic sine waves with control on amplitude and frequency. The frame is mounted on the shake table which induces a unidirectional horizontal motion in the direction of the frame's weaker inertia axis. During these tests the information provided by two accelerometers was used: the accelerometer installed at the 4th floor, where the largest displacements occurred for the first mode of vibration of the structure and therefore the floor at which the TLDs are installed, and the accelerometer placed on the shaking table to measure the input acceleration for the model steel frame.

To evaluate the behaviour of the frame and the effectiveness of the various TLD configurations at different amplitudes of base excitation, two sine waves having two different constant amplitudes in acceleration were employed. These excitations cover a frequency range of ±15 % relative to the first mode of the vibration frequency of the frame, in steps of minimum 0.01 Hz and maximum 0.05 Hz. For the un-equipped frame, the steps were kept at 0.01 Hz at frequencies ±2.5 % of its first natural frequency, and lowered to 0.05 Hz for the rest of the frequency band considered. When the frame was equipped with the different TLDs, the steps were all kept at 0.01 Hz.

The maximum amplitude configuration, "Amplitude = 100 %" (A100), was set to prevent frame yielding. The largest displacement of the top floor was limited to 13.5 mm, which derives from a constant amplitude in the acceleration wave of 0.0316 m/s^2. For the same frequency range, the amplitude was reduced to "Amplitude 25 %" (A25). Accordingly, its constant amplitude was 0.0079 m/s^2.

Each amplitude case and single frequency from the frequency bandwidth studied were evaluated individually. The duration of the forced vibration was set in order to achieve steady state behaviour based on the outcome of some preliminary tests. Adjusting the frequencies and amplitudes of the imposed displacement on the shake table is required to ensure constant amplitude across all frequencies in their corresponding acceleration waves.

Since the target frequency corresponds to the first natural frequency of the structure, two identical TLDs are located on the topmost floor of the frame (subjected to the largest displacement for the first mode of vibration) in all the amplitude, container-type, and selected-fluid conditions.

A summary of the experimental tests carried out in this work are presented in Table 7, together with the name code assigned to each. It must be noted that tests carried out with fluid M were only performed for the amplitude case A25 due to leakage over hours, making it not possible to contain the fluid for the A100 case. Tests of LCVAs with orifices were carried out for W fluid for comparison purposes of the effect of the blocking ratio.

4. Experimental results and discussion

The recorded accelerometer data has been processed using MATLAB. All the results are given for the Steady State response of the 4th floor expressed as a Frequency Response Function (FRF), which quantifies the response of a system to an external excitation, normalized by the magnitude of this excitation over a range of frequencies. In this study, the FRF is evaluated in terms of acceleration: the input corresponds to the measured acceleration induced by the shake table at base level, while the output corresponds to the acceleration recorded at the 4th floor. In the following sections, the results of the response for the un-controlled frame and the TSD and LCVA controlled frame are described in terms of modulus of the FRF.

Fig. 15 shows the experimental setups for the un-controlled frame and the TSD and LCVA controlled structure.

Table 6
Comparison of the different numerical definitions, experimental and target LCVA frequencies.

L_V (mm)	Hitchcock et al. (Hz)	Chang and Hsu (Hz)	Chaiviriyawong et al. (Hz)	Eqn. (22) (Hz)	Experimental frequency (Hz)	Target frequency (Hz)
20	1.88	2.00	2.11	2.27	2.25	2.00
25	1.82	1.93	2.02	2.16	2.19	
30	1.76	1.86	1.94	2.07	2.07	
34	1.72	1.81	1.88	2.00	2.01	
35	1.71	1.80	1.87	1.98	2.01	
40	1.66	1.74	1.81	1.91	1.94	
50	1.57	1.64	1.70	1.78	1.82	

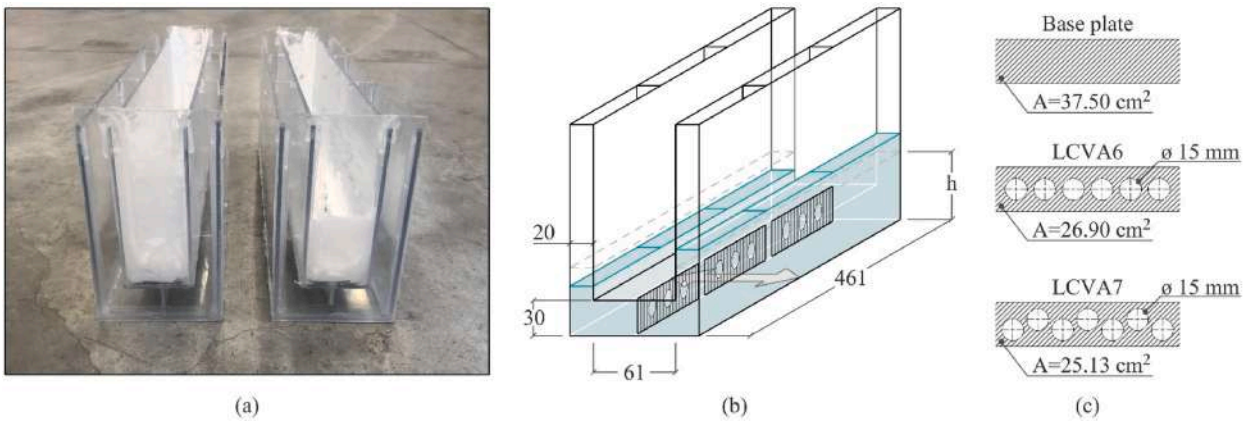

Fig. 14. LCVA with perforated barriers used in the experimental tests, specific dimensions.

Table 7
Compilation of the experimental tests.

	Un-controlled	Controlled				
	FRAME	Fluid	TSD	LCVA	LCVA6	LCVA7
Amplitude 25 %	FRAME-A25	W	TSD-W-A25	LCVA-W-A25	LCVA6-W-A25	LCVA7-W-A25
		D	TSD-D-A25	LCVA -D-A25	–	–
		M	TSD-M-A25	LCVA-M-A25	–	–
Amplitude 100 %	FRAME-A100	W	TSD-W-A100	LCVA-W-A100	LCVA6-W-A100	LCVA7-W-A100
		D	TSD-D-A100	LCVA-D-A100	–	–

Fig. 15. Experimental setups: (a) un-controlled frame, (b) TSD controlled frame, (c) LCVA controlled frame.

4.1. Frame response

The setup of FRAME-A25 and FRAME-A100 tests is shown in Fig. 15a. The structure is mounted on the shake table that induces a horizontal base motion along the frame's weaker inertia axis. The steady state Frequency Response Function (FRF) response in terms of acceleration of the 4th floor of the uncontrolled frame is depicted in Fig. 16 for both A25 and A100. The marks on the curves indicate actual experimental measurements.

The data reveals that the first natural frequency falls within the values 2.01 Hz and 2.02 Hz, as expected. It is also noticeable that the modulus of the FRF is larger in the A25 case, reaching a value of 1.99, compared to A100, which attains a value of 1.04. Table 8 provides a summary of these results. This difference in the FRF modulus values between amplitudes evidences that the empirical structural damping reflects an amplitude-dependency. Larger excitation amplitudes result in greater structural displacement which leads to a corresponding rise in the structural damping, thus the smaller FRF peak response. In this case, where no yielding occurs, larger energy dissipation may be due to the behaviour of the connections.

4.2. Frame response when equipped with TSDs

The analysis of the response of the TSD equipped frame is presented in this section. Its setup can be seen in Fig. 15b. The sloshing occurs in the containers' shortest length to obtain the desired frequency tuning. The Steady State FRF response in terms of acceleration of the 4th floor of the frame controlled with TSDs is illustrated in Fig. 17, for both A25 and A100 cases. A detailed graph can be found in Fig. 18. The fluid used is also represented. An overview of the results can be found in Table 9.

For the case TSD-W-A25, the response magnitude of the 1st frequency (1.83 Hz) has a value of 0.63, while for the 2nd one (2.22 Hz) is 0.24. This means that when the studied frame is equipped with the TSDs and the fluid in use is fluid W, the overall maximum response is reduced by 68.43 %. At resonance it is minimized by 99.50 %.

The study case TSD-D-A25 presents an absolute FRF value of 0.32 at frequency 1.82 Hz and 0.09 at 2.22 Hz. Consequently, a reduction of 84.01 % of the maximum value is observed. Again, the largest reduction is found at resonance with a response diminished by 99.55 %.

TSD-M-A25 test results in a 0.44 absolute FRF peak at 1.82 Hz. A second peak is found at 2.16 Hz with a value of 0.20. In this case, the maximum FRF experiences a 77.83 % reduction. As in the previous cases, the best reduction value is located at resonance, with a response 99.55 % smaller than for an un-controlled frame.

Observing the data yielded by test TSD-W-A100, a maximum reduction of 50.34 % of the response is evident. The first resonant peak, positioned at 1.81 Hz, exhibits an FRF value of 0.53, whereas the second peak (2.19 Hz) registers an FRF value of 0.28. In this case, the best behaviour implies a 99.13 % reduction, and it is found at resonance, as expected.

Lastly, the first natural frequency in test TSD-D-A100 is identified at 1.81 Hz and displays an FRF value of 0.24, while the second can be found at 2.19 Hz and has a value of 0.08, which implies that the maximum response reduction is 77.66 %. In accordance with the theory, the reduction at resonance is the largest (99.04 %).

From the results, it is clear that the incorporation of TSDs drastically improves the frame performance against vibrations.

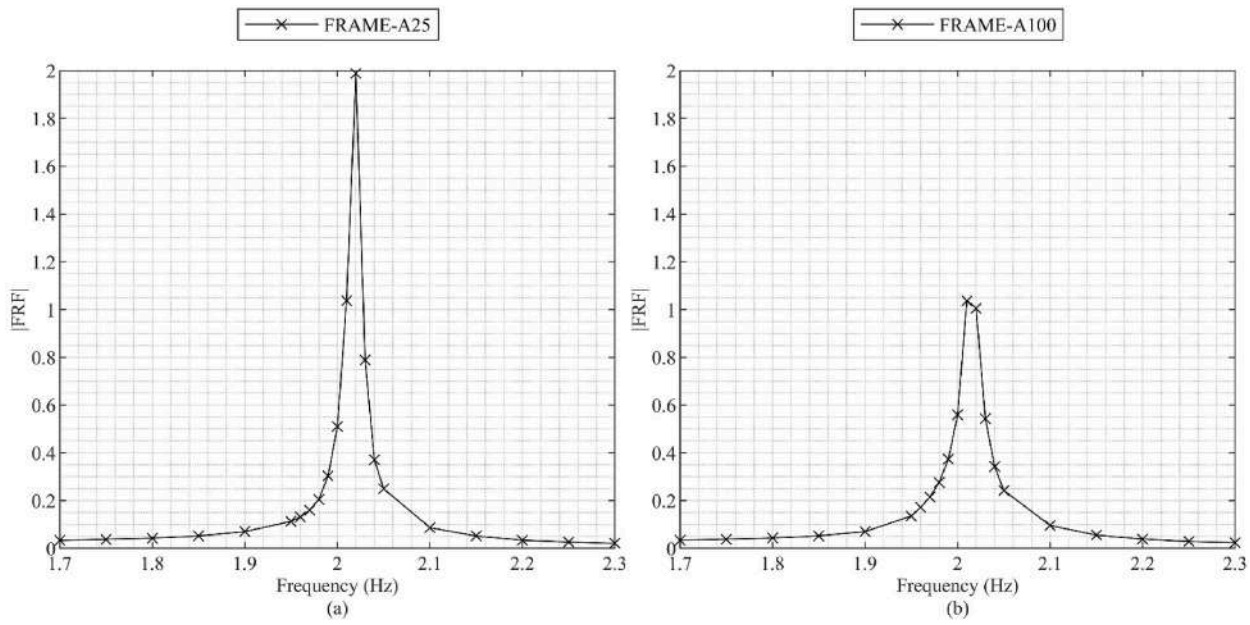

Fig. 16. Steady State response of 4th floor of the un-controlled frame: FRF in acceleration - Excitation frequency, (a) Amplitude = 25 % (b) Amplitude = 100 %.

Table 8
Frame experimental tests: natural frequency and 4th floor Steady State FRF response in acceleration.

Test name	f1 (Hz)	|FRF|
FRAME-A25	2.02	1.989
FRAME-A100	2.01	1.037

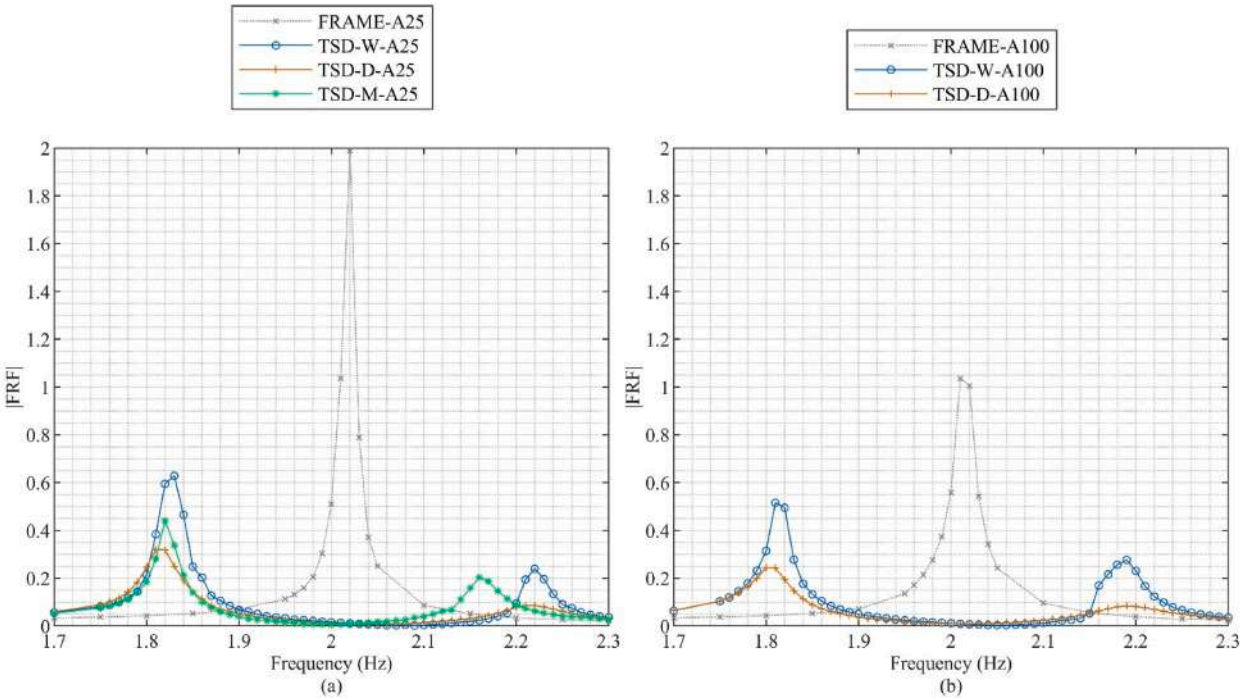

Fig. 17. Comparison of the Steady State response of 4th floor with an un-controlled and a TSD-controlled frame: FRF in acceleration - Excitation frequency, (a) Amplitude = 25 % (b) Amplitude = 100 %.

Particularly, the application of the most viscous fluid (D), leads to the largest maximum response reduction in the two acceleration scenarios, followed by utilizing fluid M and lastly, fluid W, coinciding with the lowest inherent viscosity. It is also worth noting that the order of magnitude is similar fluid-to-fluid independently of the value of acceleration considered. This implies that the control performance of TSDs decreases if the input loading increases. These results align with the work described by Chang and Hsu [28].

4.2.1. TSD surface tracking

Video tracking is carried out for frequency and wave surface elevation (η) control for the case A100. The fluid displacement in case A25 was too small to measure with video tracking, although it can be stated that continuous free surface condition was satisfied and no wave breaking occurred. The maximum TSD fluid displacement for three significant frequencies (1.80 Hz, 2.00 Hz and 2.20 Hz) is displayed in Figs. 19 and 20 and summarized in Table 10.

It was observed that for TSD-W-A100, free surface motion suffered from wave breaking on frequencies around 1.80 Hz, reaching a maximum $\eta = 46.6$ mm. In contrast, when fluid D was used, the wave breaking was suppressed for the whole frequency range considered and the maximum wave surface elevation was reached at 1.80 Hz and has a value of $\eta = 23.6$ mm, 49.4 % smaller. Near resonance, the wave surface elevation in both cases reaches very similar values of the same order of magnitude. At a frequency near the second response peak, f = 2.20 Hz, the maximum surface wave elevation was $\eta = 10.9$ mm for TSD-W-A100 and $\eta = 6.3$ mm for TSD-D-A100, 42.2 % smaller. These results are coherent with the literature: the wave amplitude decreases as the viscosity of the liquid increases [14].

This suggests that, together with the previous FRF results, the viscosity of the fluid not only achieves a better control of the structure but also allows for greater control over the fluid behavior.

4.3. Frame response when equipped with LCVAs

The use of LCVAs to mitigate the frame response is presented in this section. Fig. 15c is representative of its setup. Figs. 21 and 23

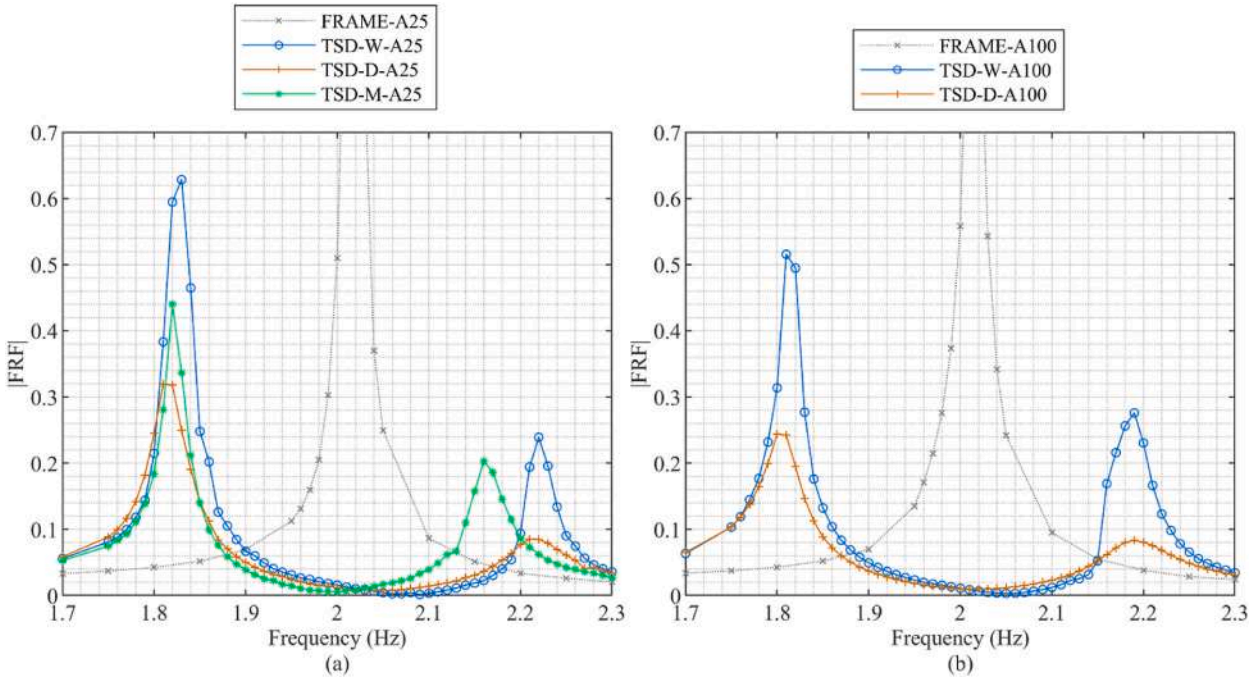

Fig. 18. Detail of comparison of the Steady State response of 4th floor with an un-controlled and a TSD-controlled frame: FRF in acceleration - Excitation frequency, (a) Amplitude = 25 % (b) Amplitude = 100 %.

Table 9
TSD experimental tests: natural frequencies, corresponding 4th floor Steady State FRF response in acceleration and response reduction percentages.

Test name	f1 (Hz)	$\|FRF\|_1$	f2 (Hz)	$\|FRF\|_2$	Maximum response reduction	|FRF| at resonance	Response reduction at resonance
TSD-W-A25	1.83	0.628	2.22	0.239	68.43 %	0.010	99.50 %
TSD-D-A25	1.82	0.318	2.22	0.085	84.01 %	0.009	99.55 %
TSD-M-A25	1.82	0.441	2.16	0.203	77.83 %	0.009	99.55 %
TSD-W-A100	1.81	0.516	2.19	0.276	50.34 %	0.009	99.13 %
TSD-D-A100	1.81	0.242	2.19	0.083	77.66 %	0.010	99.04 %

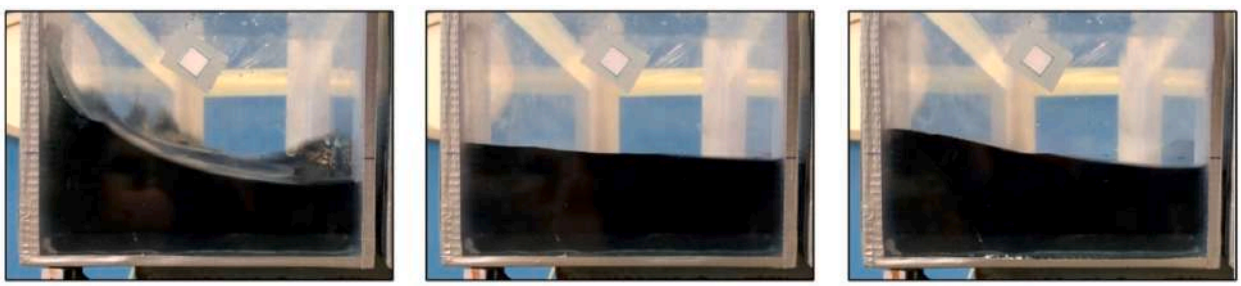

Fig. 19. TSD (fluid W) maximum wave surface elevation for different frequencies. Case Amplitude = 100 %.

depict the Steady State FRF response in terms of acceleration of the 4th floor of the frame controlled with LCVAs without orifices and with orifices respectively, utilizing different fluids and for both A25 and A100 cases. Detailed graphs can be found in Fig. 22 and Fig. 24. Table 11 gathers these results.

In the case of LCVA-W-A25, the 1st frequency is located at 1.89 Hz and its response magnitude has a value of 0.32. The 2nd frequency lies at 2.11 Hz and its response is 0.09. Therefore, the frame equipped with water based LCVAs observes a response reduction of 83.71 %. The best reduction value is located at resonance, being the response 98.69 % smaller than for an un-controlled frame.

LCVA-D-A25 test presents a single FRF peak at 1.93 Hz with an FRF value of 0.16. In this case, the maximum FRF experiences a

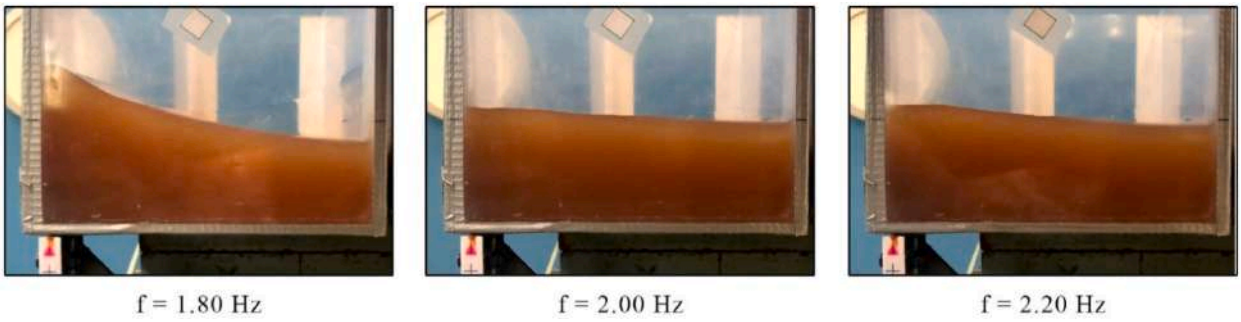

Fig. 20. TSD (fluid D) maximum wave surface elevation for different frequencies. Case Amplitude = 100 %.

Table 10
TSD maximum wave surface elevation.

	Test name	f = 1.80 Hz	f = 2.00 Hz	f = 2.20 Hz
η (mm)	TSD-W-A100	46.6	4.9	10.9
	TSD-D-A100	23.6	5.0	6.3

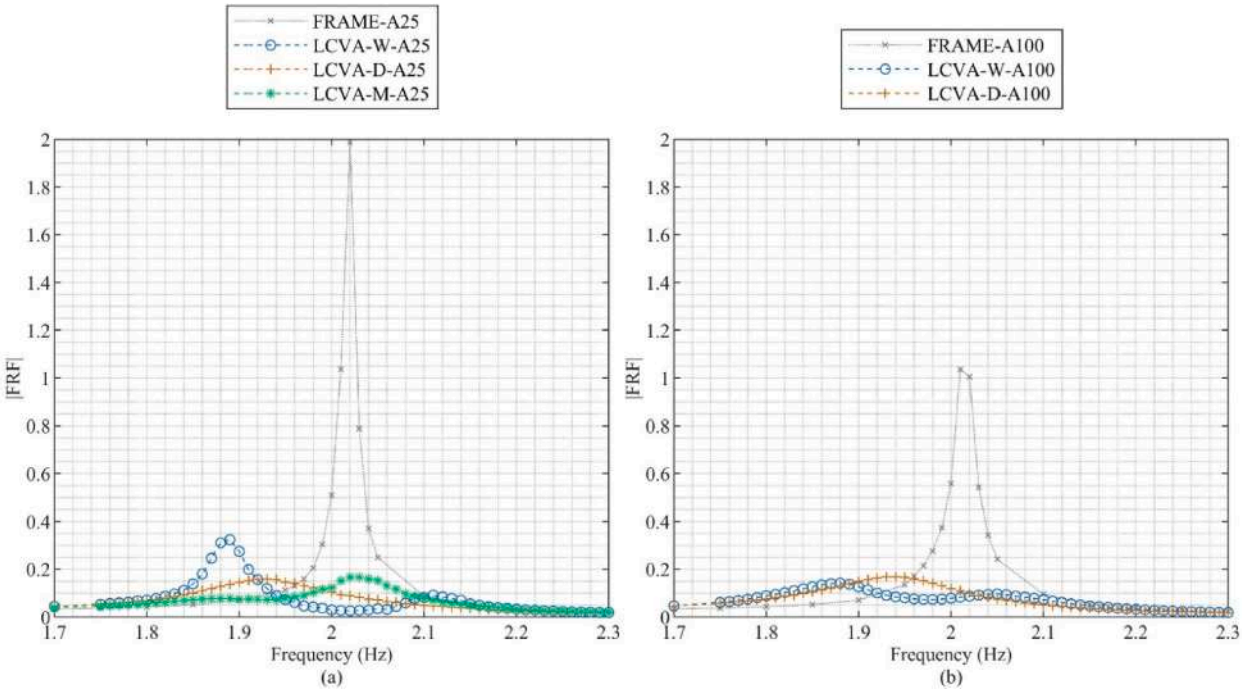

Fig. 21. Comparison of the Steady State response of 4th floor with an un-controlled and a LCVA-controlled frame: FRF in acceleration - Excitation frequency, (a) Amplitude = 25 % (b) Amplitude = 100 %.

92.01 % reduction. At resonance it is minimized by 95.53 %.

The case study LCVA-M-A25 reveals its first frequency at 1.88 Hz with a 0.08 value, smaller than the 0.167 FRF obtained at the 2nd frequency (2.03 Hz). In this case, the maximum and resonance reduction are similar: 91.60 % and 91.65 % respectively.

Shifting to the largest amplitude, test LCVA-W-A100 has a maximum response of 0.14 at 1.88 Hz. The second frequency, of 2.05 Hz, presents an FRF response of 0.10. In this case, the maximum FRF diminishes by 86.31 % while at resonance is decreased by 92.00 %.

When fluid D is used in test LCVA-D-A100, a single peak is found at 1.94 Hz, which represents a percentual reduction of 83.80 %. At resonance, the response is 89.39 % smaller compared to the un-controlled structure.

The inclusion of holes in the middle section of the LCVAs reveals that, for case LCVA6-W-A25, two peaks are formed around resonance. They are located at 1.91 Hz and 2.13 Hz and present FRF values of 0.33 and 0.06 respectively, which indicates that the

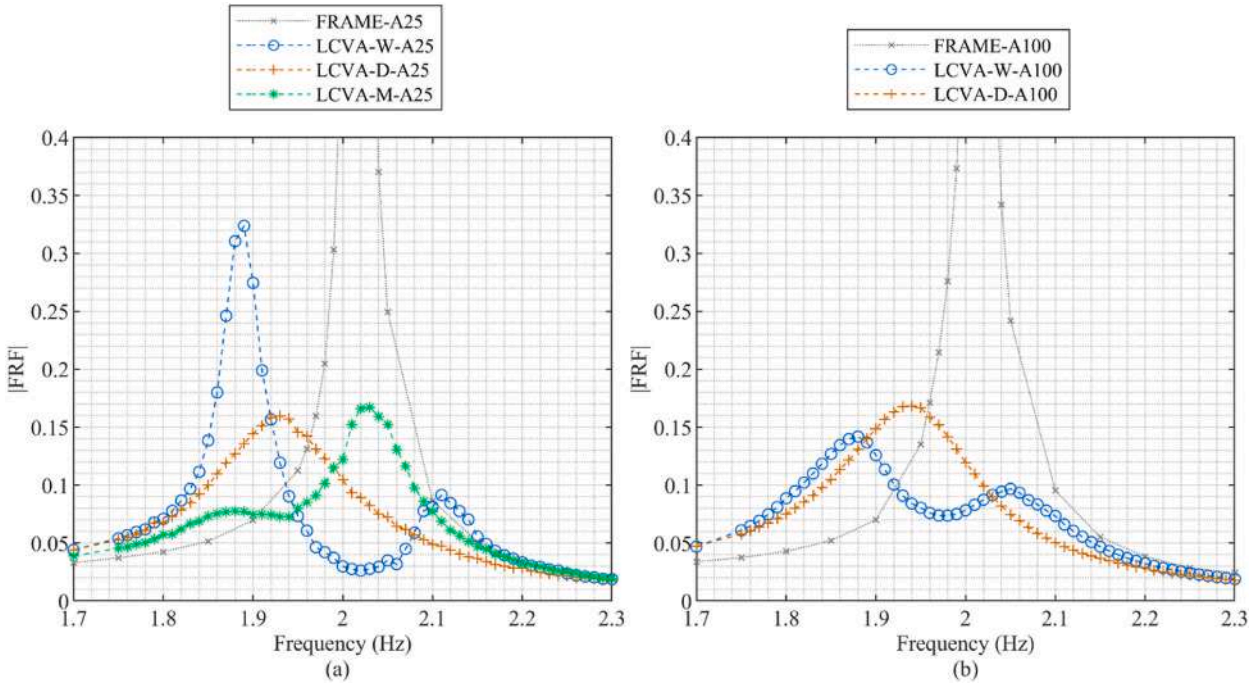

Fig. 22. Detail of comparison of the Steady State response of 4th floor with an un-controlled and a LCVA-controlled frame: FRF in acceleration - Excitation frequency, (a) Amplitude = 25 % (b) Amplitude = 100 %.

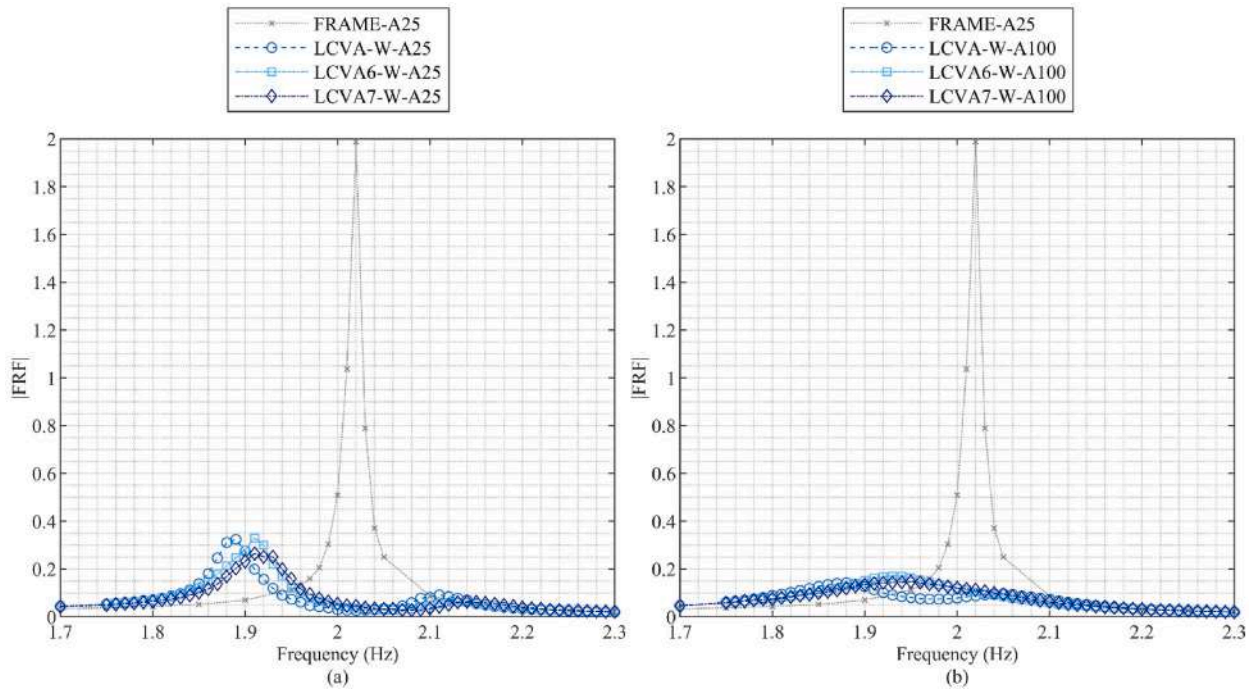

Fig. 23. Comparison of the Steady State response of 4th floor with an un-controlled and a LCVA-controlled frame for different opening configurations: FRF in acceleration - Excitation frequency, (a) Amplitude = 25 % (b) Amplitude = 100 %.

maximum peak is diminished by 83.46 %. At resonance there is a 98.19 % decrement. The new frequencies derived from LCVA7-W-A25 test can be found at 1.91 Hz and 2.14 Hz and each has a FRF response of 0.26 and 0.06. The overall maximum and resonance response reductions are 86.73 % and 97.74 % of the un-controlled frame FRF.

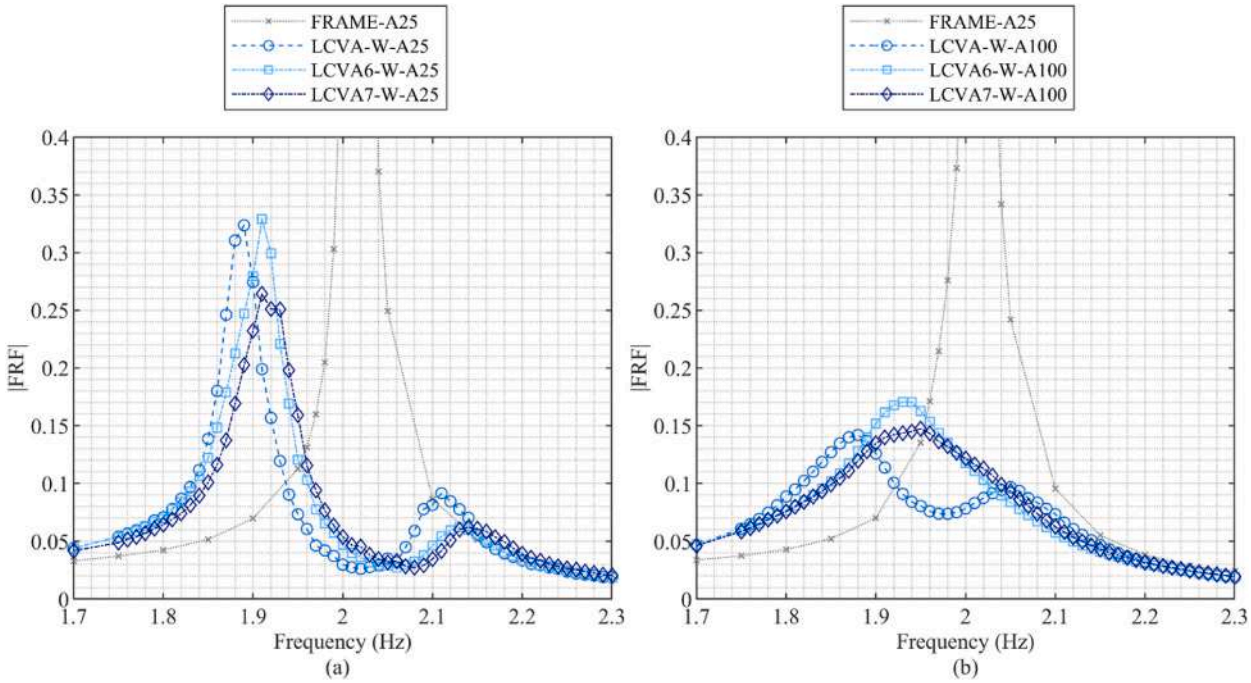

Fig. 24. Detail of comparison of the Steady State response of 4th floor with an un-controlled and a LCVA-controlled frame for different opening configurations: FRF in acceleration - Excitation frequency, (a) Amplitude = 25 % (b) Amplitude = 100 %.

Table 11
LCVA experimental tests: natural frequencies, corresponding 4th floor Steady State FRF response in acceleration and response reduction percentages.

Test name	f1 (Hz)	$\|FRF\|_1$	f2 (Hz)	$\|FRF\|_2$	Maximum response reduction	|FRF| at resonance	Response reduction at resonance
LCVA-W-A25	1.89	0.324	2.11	0.092	83.71 %	0.026	98.69 %
LCVA-D-A25	1.93	0.160	–	–	92.01 %	0.089	95.53 %
LCVA-M-A25	1.88	0.077	2.03	0.167	91.60 %	0.166	91.65 %
LCVA6-W-A25	1.91	0.329	2.13	0.062	83.46 %	0.036	98.19 %
LCVA7-W-A25	1.91	0.264	2.14	0.062	86.73 %	0.045	97.74 %
LCVA-W-A100	1.88	0.142	2.05	0.097	86.31 %	0.083	92.00 %
LCVA-D-A100	1.94	0.168	–	–	83.80 %	0.110	89.39 %
LCVA6-W-A100	1.93	0.171	–	–	83.51 %	0.111	89.30 %
LCVA7-W-A100	1.95	0.147	–	–	85.82 %	0.116	88.81 %

The results yielded for the largest of amplitudes reveal that LCVA6-W-A100 couples into a single peak of 0.17 at 1.93 Hz, reducing the maximum response by 83.51 %. At resonance, the FRF response is diminished by 89.30 %. In the LCVA7-W-A100 case, the frequency is located at 1.95 Hz and shows a response of magnitude 0.15, reducing the maximum by 85.82 %. In this case, a decrement of 88.81 % is found at resonance.

The effectiveness of LCVAs is evident from these results. It must be pointed out that the inherent damping of LCVAs configuration, together with higher viscosity of fluids D and M, results in a single-peak response curve, coherent with damping over the optimum value [14] (see Section 2). This is evident in both A25 and A100 cases. Instead, when the liquid is water, a two-peak response curve is observed which also provides the maximum reduction at resonance.

In this case, the fluid-to fluid response does vary significantly with the base amplitude for LCVA-W tests, in which damping is seen to increase together with the amplitude, while LCVA-D tests, in which the most viscous fluid is applied, produce similar results despite the amplitude.

Focusing on the behaviour of water-based LCVAs with different orifice configurations, it can be seen that the inclusion of blocking in the horizontal section increases the damping. This is particularly clear observing the LCVA6-W and LCVA7-W in comparison to LCVA-W. Moreover, for this particular case, the smaller blocking ratio obtained in the LCVA7-W configuration yields a slightly smaller maximum FRF response, compared to LCVA6-W.

It is also worth noting that the same level of performance can be obtained either by utilizing fluid D LCVAs or fluid W LCVA6 and LCVA7 configurations in the case of amplitude A100. This implies that the damping can be similarly controlled by means of increasing the liquid viscosity or with the inclusion of perforated screens that modify the head loss parameter in the horizontal section.

4.3.1. LCVA surface tracking

The maximum fluid column height is evaluated through surface video tracking for case A100 and is depicted in Figs. 25–27 and 28 for three characteristic LCVA frequencies (1.90 Hz, 2.00 Hz and 2.10 Hz). Again, the fluid displacement in case A25 was too small to measure with video tracking; however, it can be stated that the fluid movement satisfied the continuous free surface condition for the whole range considered.

In the amplitude A100 tests the largest fluid displacements occur at 1.90 Hz for all the tests evaluated. The effect of fluid viscosity can be seen by comparison between LCVA-W-A100 and LCVA-D-A100. In the first case, the maximum fluid displacement is 8.68 mm while in the second case it is reduced to 8.25 mm. The effect of the perforated screen inclusion can be derived from comparison between LCVA-W-A100, LCVA6-W-A100 and LCVA7-W-A100. It must be noted that in this case, only from visual inspection there is no significant control of the fluid motion when the screens are added.

4.4. Comparison of the TSD-LCVA response

All the case studies developed in this work are brought together in Fig. 29 for comparison.

In A25 tests, it is clear from the figure that the effective mass was larger in TSD tanks than in LCVA recipients, since the former results show response reduction for a wider frequency band. The increment in fluid viscosity shows an improvement in the behaviour for TSDs; the opposite occurs for the LCVAs considered in the present study. It is also worth noting that a similar level of FRF reduction can be obtained through TSD-D-A25 and LCVA-W-A25, with the main difference residing in the frequency bandwidth in which the devices are effective which is directly related to the amount of effective mass of the TLDs.

The influence of large amplitudes is clear from A100 tests, in which the best behaviour was obtained from TSD-D-A100, showing again an improvement of the response for high viscosity fluids when TSDs are employed. It is also worth mentioning that extremely similar results are obtained for LCVA-D-A100, LCVA6-W-A100 and LCVA7-W-A100, which means that both the fluid viscosity and the fluid passage through blocking screens can be used to increase the device's damping.

5. Numerical simulation

This section describes the numerical model developed to represent the studied frame and TLDs and to support the interpretation of the experimental results. The widely used open-source software framework OpenSees has been used to create the numerical model and carry out the analyses. The following sections include the description of the Finite Element (FE) model of the frame, the model updating process performed to adjust some of its parameters based on the measurements obtained experimentally for calibration, together with the description of the FE model to include the TLDs studied in this work.

5.1. Description of the frame FE model

The frame is defined by means of a bi-dimensional FE model, depicted in Fig. 30. The node connections between elements are considered as rigid. The slabs and columns are defined with elastic beam-column elements. Different beam-column elements are used to model the end regions of the columns, where angle profiles are present to provide connection with the slabs. The stiffness of these elements is scaled by a different factor for each floor (kkAng0 … kkAng4), set by means of the model updating procedure described in the following section (Model updating). The nodes at the base are considered fixed. The masses corresponding to the structure plus the lumped masses have all been added, in the corresponding proportion, at the nodes that connect the beam slab with the columns. For this study, the mass of the accelerometers (1.20 kg per piece) on the 4^{th} and 3^{rd} floors is included. Damping of the frame is modelled using Rayleigh damping, considering modes 1 and 4.

5.1.1. Model updating

Model updating has been performed to adjust the parameters (kkAng0 … kkAng4) that define the stiffness of the end elements of each column, to represent the presence of the angular connectors. The procedure adopted is based on the optimization of a cost

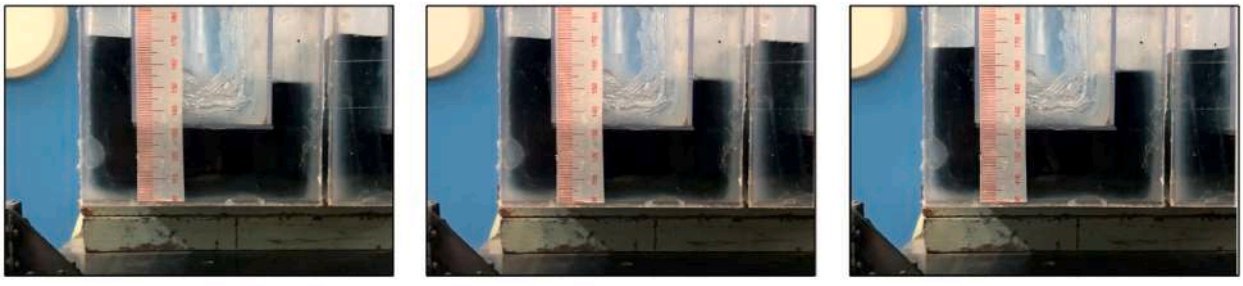

Fig. 25. LCVA (fluid W) maximum wave surface elevation for different frequencies. Case Amplitude = 100 %.

Fig. 26. LCVA (fluid D) maximum wave surface elevation for different frequencies. Case Amplitude = 100 %.

Fig. 27. LCVA6 (fluid W) maximum wave surface elevation for different frequencies. Case Amplitude = 100 %.

Fig. 28. LCVA7 (fluid W) maximum wave surface elevation for different frequencies. Case Amplitude = 100 %.

function defined as the summation of two terms (Eqn. (23)).

$$C = C_1 + C_2 \tag{23}$$

The first component of the cost function (C_1) (Eqn. (24)) measures the discrepancy between the experimentally obtained frequencies and the ones resulting from the numerical modal analysis, denoted by f^{exp} and f^{num} respectively.

$$C_1 = \sum_{i=1}^{4} \left(\frac{f_i^{num} - f_i^{exp}}{f_i^{exp}} \right)^2 \tag{24}$$

where *i* indicates the number of the mode of vibration.

The second component of the cost function (C2) (Eqn. (25)) measures the difference between the experimental and numerical mode shapes (Φ^{exp} and Φ^{num} respectively) by utilizing the Modal Assurance Criterion (MAC), which calculates the correlation between the two vibration shapes.

$$C_2 = \sum_{i=1}^{4} \left(1 - MAC\left(\Phi_i^{num}, \Phi_i^{exp}\right)\right) \tag{25}$$

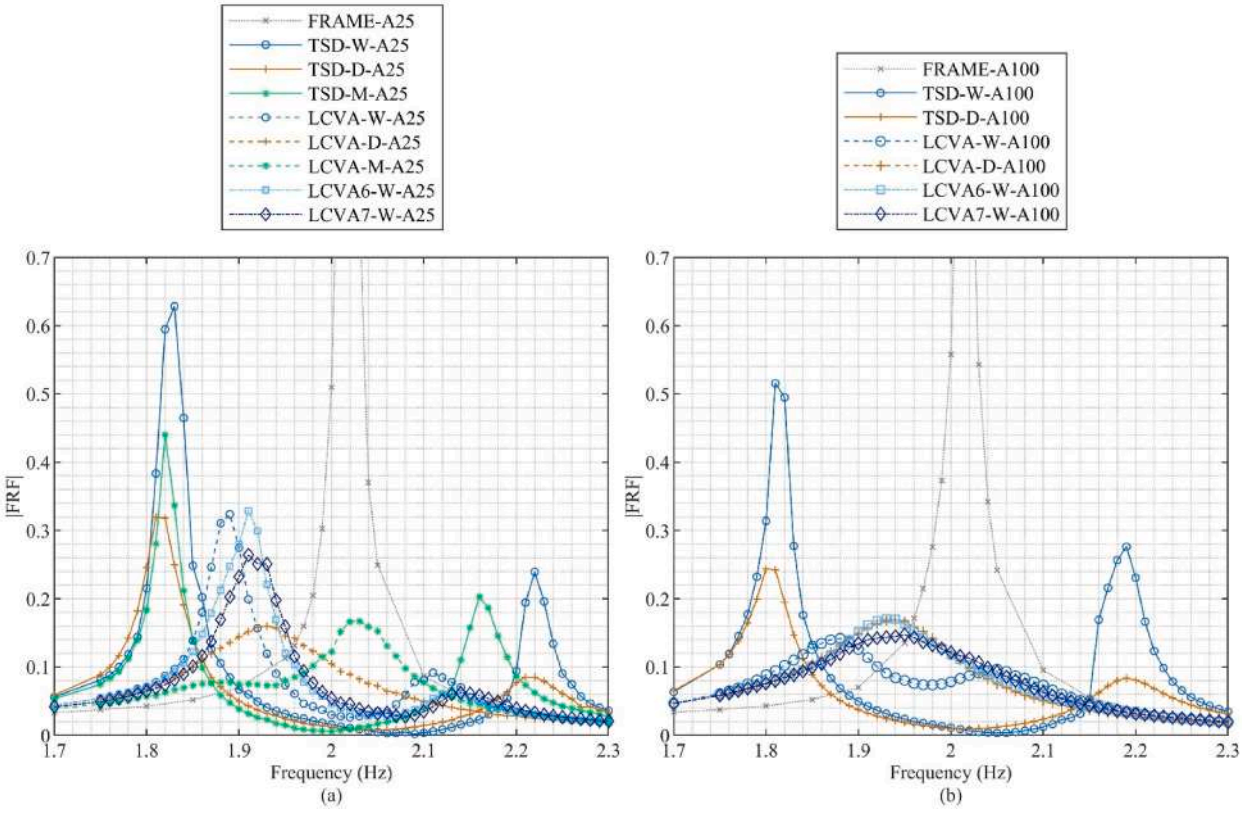

Fig. 29. Comparison of the Steady State response of 4th floor when equipped with TSDs or LCVAs: FRF in acceleration - Excitation frequency, (a) Amplitude = 25 % (b) Amplitude = 100 %.

The optimization carried out considers various scenarios in which different weights are given to each natural frequency (WNF = [f_1 f_2 f_3 f_4]) and mode number (WMN = [Φ_1 Φ_2 Φ_3 Φ_4]) so that each mode participation can be evaluated individually in the search of accurate results. Some examples that illustrate how the minimum values, represented with the darkest blue, of the cost functions C_1 and C_2 vary are shown in Fig. 31 for combinations of kkAng1 … kkAng4 with equal assignments of the weights for all modes: WNF = [1 1 1 1] and WMN = [1 1 1 1]. It can be seen that the values required to minimize C_1 and C_2 occur in different regions. For this reason, different weight combinations have been studied. The outcome of the model updating of three characteristic examples (tests PA, PB and PC) is displayed in Table 12 together with their corresponding natural frequencies. The values selected to define the FE model derive from test PA, which provides the best results in terms of frequencies, essential for the tuning of the TLDs. Table 13 provides a side-by-side comparison of the modal shapes obtained experimentally (Φ_i^{exp}) and numerically (Φ_i^{num}) with the parameters extracted from test PA, while Fig. 32 graphically illustrates these results.

The effective modal masses (M_i^*) of the frame with the supplementary lumped mass on each storey are obtained from Equation (26) [72,73]. They are dependent on the lumped masses (m_i), mode shape (Φ_i) and modal participation factor (Γ_i) defined in Equation (27). The modal participation factors, the effective modal masses, and their percentage with respect to the total mass are displayed in Table 14.

$$M_i^* = \Gamma_i \sum m_i \Phi_i \tag{26}$$

$$\Gamma_i = \frac{\sum m_i \Phi_i}{\sum m_i \Phi_i^2} \tag{27}$$

5.2. Description of the TLDs FE model

The bi-dimensional FE model of the frame was updated to include the modelling of two TLDs on the 4th floor, as depicted in Fig. 33. For each TLD, the node in height with the slab (S-4) includes the non-effective mass (m_0) and the container mass (m_{cont}). An auxiliary node (TLD-aux) is placed at a height h_1, which represents the height at which the centre of the effective mass is located. The command equalDOF is used to construct a constraint between TLD-aux and S-4 for all 3 DOFs. The node named TLD is used to apply the effective mass (m_1). It is positioned at the same location as TLD-aux with the use of zeroLength elements, that include the uniaxial elastic

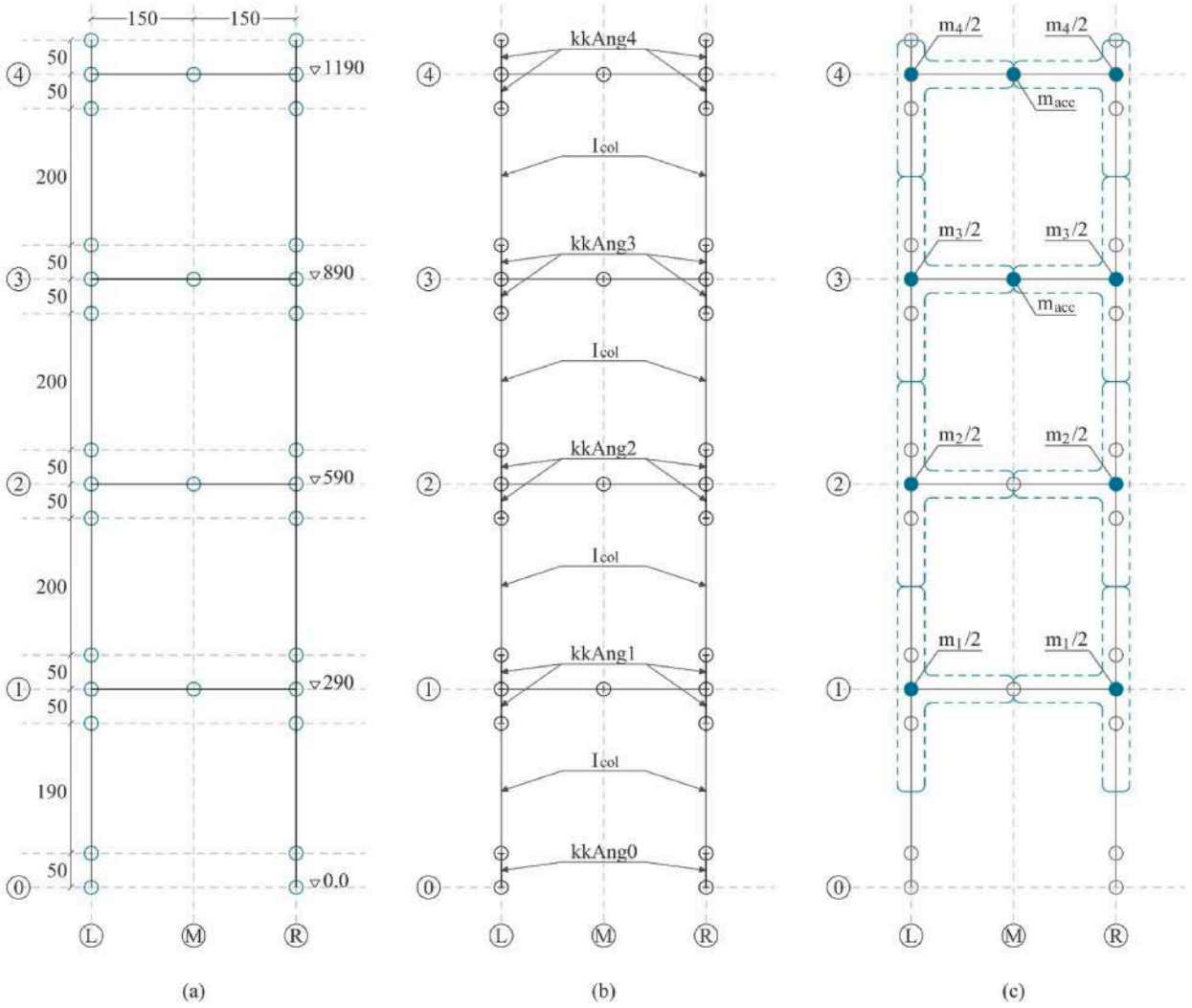

Fig. 30. FE model of the frame: (a) dimensions in mm, (b) elements: columns and kkAng0-4 column sections (c) mass assignments.

material for the spring with stiffness k_1 and uniaxial viscous material to represent the damper with damping c_1. The fix command is used to impose constraints on the vertical movement and rotation, ensuring the displacement occurs only in the horizontal direction.

5.3. *Overview of the numerical analyses*

The numerical time history analysis procedure has followed the experimental scheme: the same unidirectional constant-amplitude harmonic waves described in Section 3.3 have been applied at the base of the model for the evaluated frequency range, for both Amplitude = 25 % and Amplitude = 100 %. For reference, see Table 7.

For the definition of the parameters that characterize TLDs, four different numerical scenarios are considered for TSDs and LCVAs for comparison with the experimental results, refining the optimization on each step. On each of them, the influence on the response of the frame-absorber system of the mass ratio (μ), tuning ratio (β) and damping ratio (ξ) is clearly defined. The detailed explanation is provided below, while Table 15 gathers the summarized information.

For TSDs, the scenarios considered are as follows:

- Case N1-TSD. The masses are determined based on Equations (8) and (9), the frequency is calculated according to Equation (7) and the damping is expressed in terms of the damping ratio (ξ) as $c_1 = 2\xi m_1 \omega_1$, and considers the value recommended by Eurocode 8 [61], $\xi = 0.5$ %.
- Case N2-TSD. The damping considered is defined in Equation (11), while the rest of parameters are maintained from the previous case N1-TSD. It should be recalled that, for TSDs, wave surface elevation data could only be gathered in the amplitude A100 cases, thus making it not possible to determine the numerical value for damping in the A25 cases.

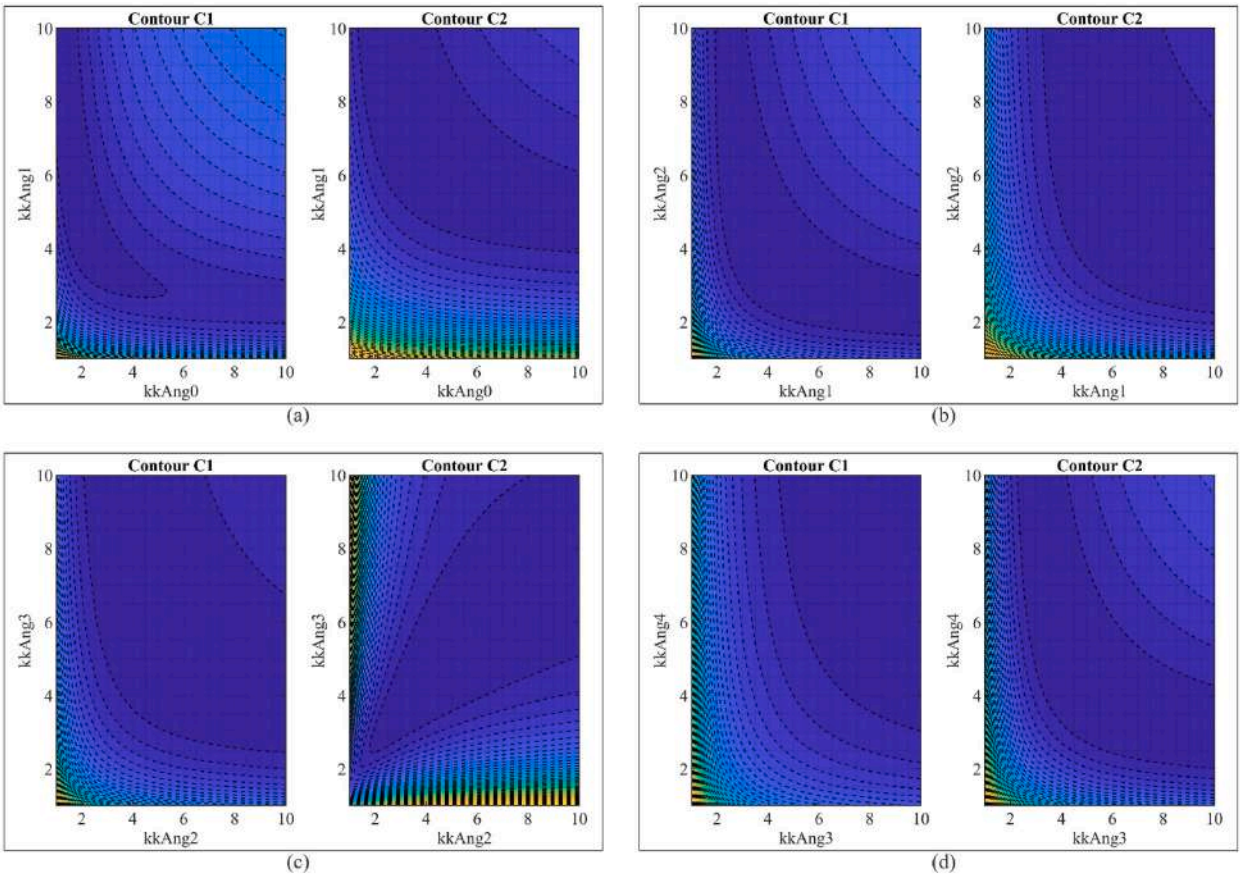

Fig. 31. Contour diagram of the minimization of the cost functions C_1 and C_2 for: (a) kkAng0-kkAng1, (b)kkAng1-kkAng2, (c) kkAng2-kkAng3 and (d) kkAng3-kkAng4.

Table 12
Model updating results of kkAng0 … kkAng4 for tests PA, PB and PC and corresponding natural frequencies.

	WNF	WMN	kk Ang0	kk Ang1	kk Ang2	kk Ang3	kk Ang4	f_1 (Hz)	f_2 (Hz)	f_3 (Hz)	f_4 (Hz)
PA	[1 1 0 0]	[0 0 0 0]	2.00	4.05	3.00	8.99	6.40	2.015	6.039	9.202	11.333
PB	[1 1 0 0]	[1 1 0 0]	3.13	3.14	3.71	4.57	6.78	2.030	5.992	9.103	11.088
PC	[1 0 0 0]	[1 0 0 0]	2.00	4.97	3.68	2.49	7.37	2.015	5.723	8.949	10.795
Target frequency								2.015	6.039	9.447	11.519

Table 13
Comparison of experimental and test PA numerical modal shapes, normalized for absolute maximum value = 1.

	Φ_1^{exp}	Φ_1^{num}	Φ_2^{exp}	Φ_2^{num}	Φ_3^{exp}	Φ_3^{num}	Φ_4^{exp}	Φ_4^{num}
Floor 4	1.00	1.00	0.87	0.88	0.53	0.62	0.39	0.48
Floor 3	0.88	0.90	0.05	0.11	−0.64	−0.64	−1.00	−1.00
Floor 2	0.63	0.69	−0.89	−0.89	−0.36	−0.59	0.97	0.85
Floor 1	ND	0.36	ND	−1.00	ND	1.00	ND	−0.44

- Case N3-TSD. A model updating has been performed to adjust the parameters of mass, frequency and damping for all amplitudes of excitation through the variables m_1, f_1 and ξ respectively. The variable for the effective mass (m_1) represents a fraction of the total fluid mass (m_{TOT}), which was obtained from the geometry of the recipient and density of the fluids and was verified experimentally. The frequency tuning is evaluated trough the frequency of sloshing of the fluid (f_1) and can be used to evaluate the prediction derived from the theoretical frequency obtained from Equation (7) since slight mistuning can arise from geometry imprecisions in the container or in its filling. Finally, the value for the damping ratio (ξ) is determined. The optimization carried out aims to

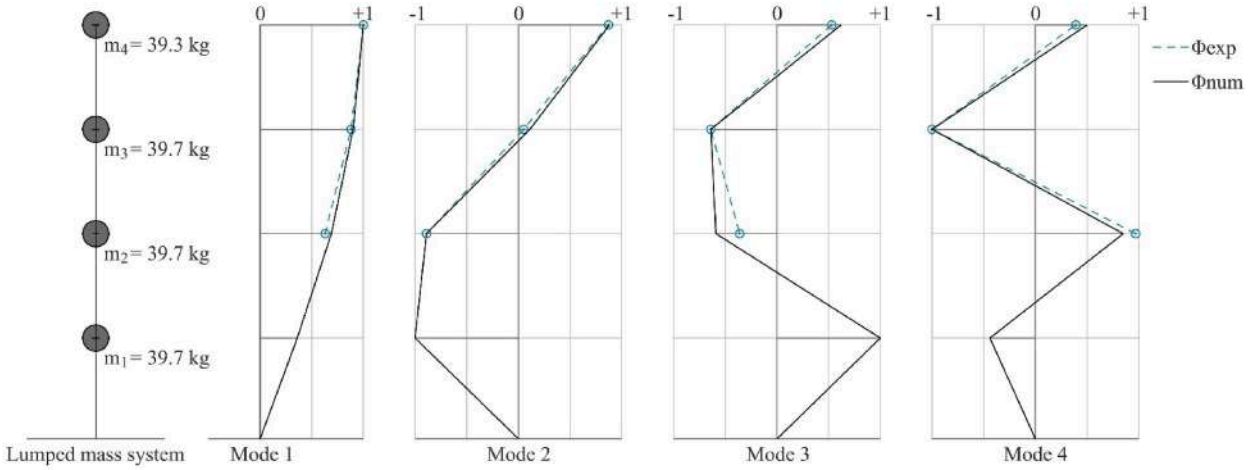

Fig. 32. Lumped mass system scheme and modal shapes (experimental and numerical results).

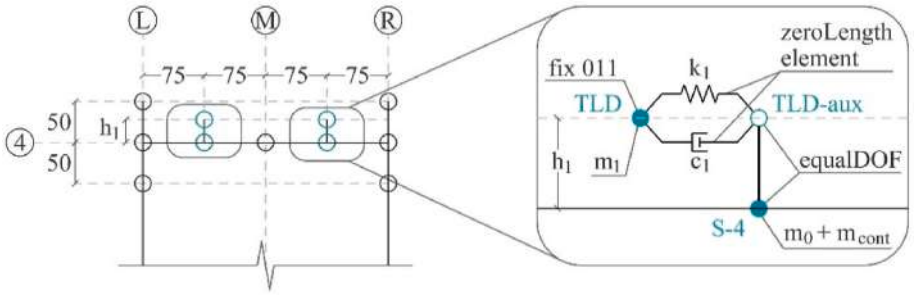

Fig. 33. Floor 4 FE model of the frame with nodes, elements and restrictions for TLDs.

Table 14
Modal participation factor, effective modal mass and ratio of effective modal mass with respect to the total mass.

	Γ_i	M_i^*	M_i^*/M_{TOT}
Mode 1	1.222	142.73 kg	89.88 %
Mode 2	−0.353	12.79 kg	8.06 %
Mode 3	0.181	2.78 kg	1.75 %
Mode 4	−0.054	0.25 kg	0.16 %

Table 15
Numerical scenarios for TSD and LCVA definition: natural frequencies, effective mass and damping ratio considerations.

Test name	Frequency (f_1)	Effective mass (m_1)	Damping Ratio (ξ)
N1-TSD	$f_{TSD,1}$ from Equation (7)	m_1 from Equation (9)	From EC-8 [61]
N2-TSD	$f_{TSD,1}$ from Equation (7)	m_1 from Equation (9)	$\xi = c_1/2m_1\omega_1$ c_1 from Equation (11)
N3-TSD	Optimised	Optimised	Optimised (constant)
N4-TSD	Optimised	Optimised	Optimised (linear)
N1-LCVA	f_{LCVA} from Equation (14) L_{eff} from Equation (22)	$m_1 = m_{TOT}$ m_{TOT} from Equation (17)	From EC-8 [61]
N2-LCVA	f_{LCVA} from Equation (14) L_{eff} from Equation (22)	m_1 = mass inside the columns	From EC-8 [61]
N3-LCVA	Optimised	Optimised	Optimised (constant)
N4-LCVA	Optimised	Optimised	Optimised (linear)

minimize the cost function (C_{FRF}), defined in Equation (28), which compares the experimentally obtained FRF values in acceleration for the Steady State response of the 4th floor (y^{exp}) with the ones resulting from the numerical modal analysis (y^{num}) for all the frequencies studied (n), which range from 1.75 Hz to 2.35 Hz, every 0.01 Hz.

- Case N4-TSD. The last approach further develops the definition of the damping ratio (ξ), which is set as a linear amplitude-dependent parameter defined by the equation of a straight line, $y = mx + n$. Both m_1 and f_1 are defined as in the previous case.

For LCVAs, the scenarios considered are as follows:

- Case N1-LCVA. The mass is set according to Equation (17) and represents the total fluid mass as effective. The frequency of the LCVA is calculated according to Equation (14), in which the value for L_{eff} is proposed by the authors in Equation (22), and the damping is expressed in terms of the damping ratio (ξ) as $c_1 = 2\xi m_1 \omega_1$, and considers the value recommended by Eurocode 8 [61], $\xi = 0.5$ %.
- Case N2-LCVA. The effective mass of the damper (m_1) is considered herein as the mass residing inside the columns to match with the studies carried out by Xu el al [24]. and Abou et al. [34], while the rest of parameters remain the same as in case N1-LCVA.
- Case N3-LCVA. Similarly to case N3-TSD, a model updating has been carried out to determine the parameters of mass, frequency and damping through the variables m_1, f_1 and ξ respectively, where m_1 is defined as a fraction of the total fluid mass which was derived from the recipient's geometry and the fluids' densities and was verified experimentally. Since minor mistuning can occur due to geometric inaccuracies in the containers or in their filling, the numerically optimised LCVA frequency (f_1) is compared to the theoretical one obtained from Equation (14) in which the value for L_{eff} is proposed by the authors as in Equation (22). Finally, the damping ratio (ξ) is also obtained. The optimization process minimizes the cost function (C_{FRF}) defined in Equation (28), which compares the experimentally obtained FRF values in acceleration for the Steady State response of the 4th floor (y^{exp}) with those from the numerical modal analysis (y^{num}) for all the frequency range (n), from 1.75 Hz to 2.35 Hz in 0.01 Hz increments.
- Case N4-LCVA. Similarly to case N4-TSD, the damping ratio (ξ) is established as a linear parameter dependent on the amplitude, defined by the equation of a straight line is $y = mx + n$, while m_1 and f_1 are set as in the previous case.

$$C_{FRF} = \sum_{i=1}^{n=61} \left(y_i^{num} - y_i^{exp}\right)^2 \tag{28}$$

6. Numerical results and discussion

Following the approach outlined in Section 4 for the experimental analysis, the results are expressed in terms of the Steady State response of the 4th floor as the FRF evaluated in the acceleration of the top floor of the model relative to its base. The following sections include the results for the un-controlled frame, as well as for the frame controlled with TSDs and LCVAs.

6.1. Frame response

The numerical frame characteristics have been detailed in Section 5.1.1. A comparison of the steady state FRF response in terms of

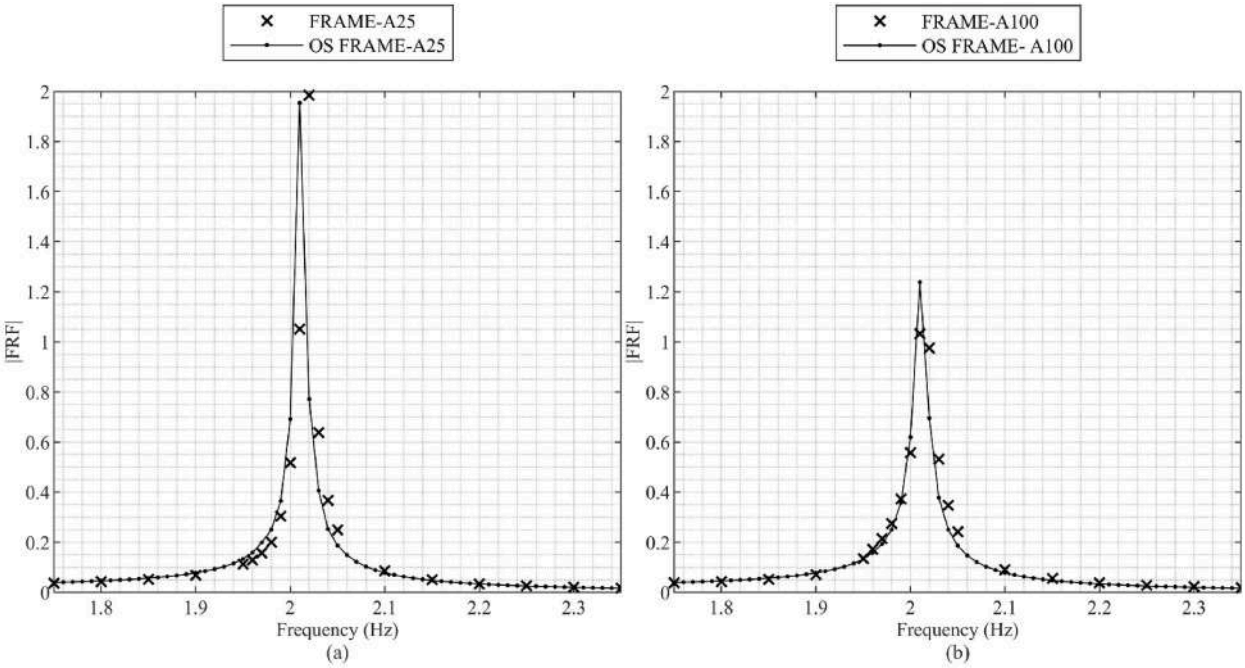

Fig. 34. Experimental and numerical FRF in acceleration of the 4th floor of frame, (a) Amplitude 25 %, (b) Amplitude 100 %.

acceleration of the 4th floor of the uncontrolled frame between the experimental results, FRAME-A25 and FRAME A-100, and the numerical analyses can be found in Fig. 34, for both A25 and A100. The damping coefficient of the model that best represents the experimental behaviour is set to $\xi = 0.18$ % for the A25 case and $\xi = 0.30$ % for the A100 scenario, which mirrors the amplitude-dependency.

6.2. Frame response equipped with TSDs

The numerically obtained response of TSDs for the four cases considered is presented in this section. A summary of the data related to frequency of sloshing (f_1), effective mass (m_1) and damping coefficient of the fluid (ξ) used for the modelling for all the simulations studied crossed with the numerical scenarios is presented in Table 16, along with the value obtained from the minimization of the cost function (C_{FRF}). It can be observed from the data that the values obtained from the cost function decrease in every step of the optimization, reaching their minimum for the N4 cases, which implies that the greatest accuracy was obtained when slight mistuning was accounted for, the effective mass reached values about 5 % smaller than expected and the damping was set as linearly dependent on the amplitude of the acceleration.

The comparison between all numerical scenarios and experimental results for the frame equipped with TSD-W response can be seen in Fig. 35. From Fig. 35a it is clear that the response prediction provided by N1 is affected by the 2.5 % over-tuning observed in the experiments, which results in discrepancies of the response peaks from 0.02 to 0.03 Hz. The optimised parameters suggest that the mass that participates in the sloshing seems to be smaller than that proposed by the literature by 2.5 %–5.0 %. Regarding the damping, the N3 numerical damping is around 50 % greater than the theoretical damping coefficient, meaning that, in this case, the recommendation available in the literature would slightly overestimate the response. The best accuracy is obtained for the linear damping scenario, N4, which takes values of 0.94 % and 0.43 % for the first and second peaks respectively, showing great agreement with the experimental campaign.

Fig. 35b demonstrates that the predictions derived from the literature are in good agreement with the experimental results. In this case, the mistuning was minimum, and the main difference lies in the consideration of the damping ratio. In this case, the value suggested by the Eurocodes is in accordance with the optimised results, which double the numerically calculated value in N2. The best approach is to consider the amplitude-dependent damping from case N4, in which the first and second peaks retrieve 0.62 % and 0.33 % damping ratios respectively. Again, the optimization procedure suggests that the effective mass is slightly smaller than the one provided in the literature.

The application of the most viscous fluid on TSDs evinces how it affects the damping coefficient. Fig. 36a highlights the overestimation of the system response if the recommended damping value in the codes is not modified. In this particular case, a damping coefficient value almost 5 times higher than expected is required for the optimised solution N3, while the linearly variable damping from N4 results in damping coefficients equal to 2.56 % and 1.71 % for the first and second response peaks respectively. The response is seen to be additionally influenced by the 1.02 % overturning, as evidenced by numerical analyses N3 and N4. The optimised solutions N3 and N4 also suggest that the effective mass is respectively from 5 % to 6 % smaller than the one defined in the literature (see Fig. 37).

It can be seen in Fig. 36b that no mistuning was detected in the large amplitude case. The prediction of the damping derived from analysis N2 is of the same order of magnitude as that returned by the optimization process N3, with both being about 5 times higher than the one suggested in the Eurocode. The best fit is however achieved by analysis N4, which results in damping coefficients of 2.72 % for the first response peak and 2.09 % for the second one. The results derived from the optimised analyses N3 and N4 suggest that the effective mass is 5 % smaller than expected.

The use of the medium-viscosity fluids is seen to have also great effect on the damping of the TSD. From Fig. 37 a minor under-

Table 16
TSD numerical analysis data.

Test name		TSD-W-A25	TSD-D-A25	TSD-M-A25	TSD-W-A100	TSD-D-A100
N1	f_1	2.02 Hz	2.02 Hz	2.02 Hz	2.02 Hz	2.02 Hz
	m_1	3.54 kg	3.84 kg	3.08 kg	3.54 kg	3.84 kg
	ξ	0.50 %	0.50 %	0.50 %	0.50 %	0.50 %
	C_{FRF}	0.8282	0.5660	0.2090	0.1101	0.2763
N2	f_1	–	–	–	2.02 Hz	2.02 Hz
	m_1	–	–	–	3.54 kg	3.84 kg
	ξ	–	–	–	0.26 %	2.15 %
	C_{FRF}	–	–	–	0.1465	0.0089
N3	f_1	2.07 Hz	2.05 Hz	2.01 Hz	2.03 Hz	2.02 Hz
	m_1	3.40 kg	3.50 kg	2.80 kg	3.27 kg	3.53 kg
	ξ	0.71 %	2.35 %	1.16 %	0.45 %	2.50 %
	C_{FRF}	0.0440	0.0027	0.0120	0.0397	0.0015
N4	f_1	2.07 Hz	2.06 Hz	2.01 Hz	2.03 Hz	2.02 Hz
	m_1	3.39 kg	3.57 kg	2.81 kg	3.28 kg	3.57 kg
	m (ξ)	0.01096	0.03390	0.01342	0.01160	0.03672
	n (ξ)	0.00170	0.01440	0.00691	1.165 e−6	0.01799
	C_{FRF}	0.0246	0.0012	0.0092	0.0250	0.0008

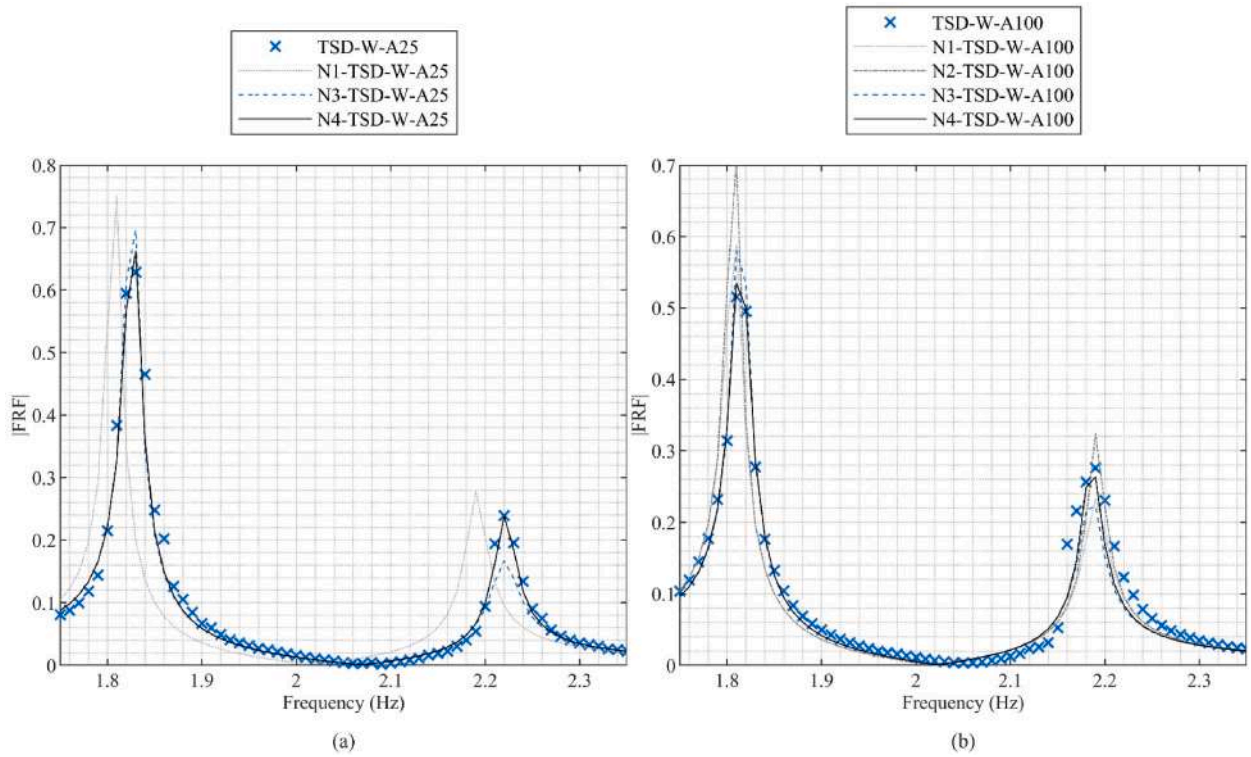

Fig. 35. Experimental and numerical FRF in acceleration of the 4th floor of frame equipped with TSD-W, (a) Amplitude 25 %, (b) Amplitude 100 %.

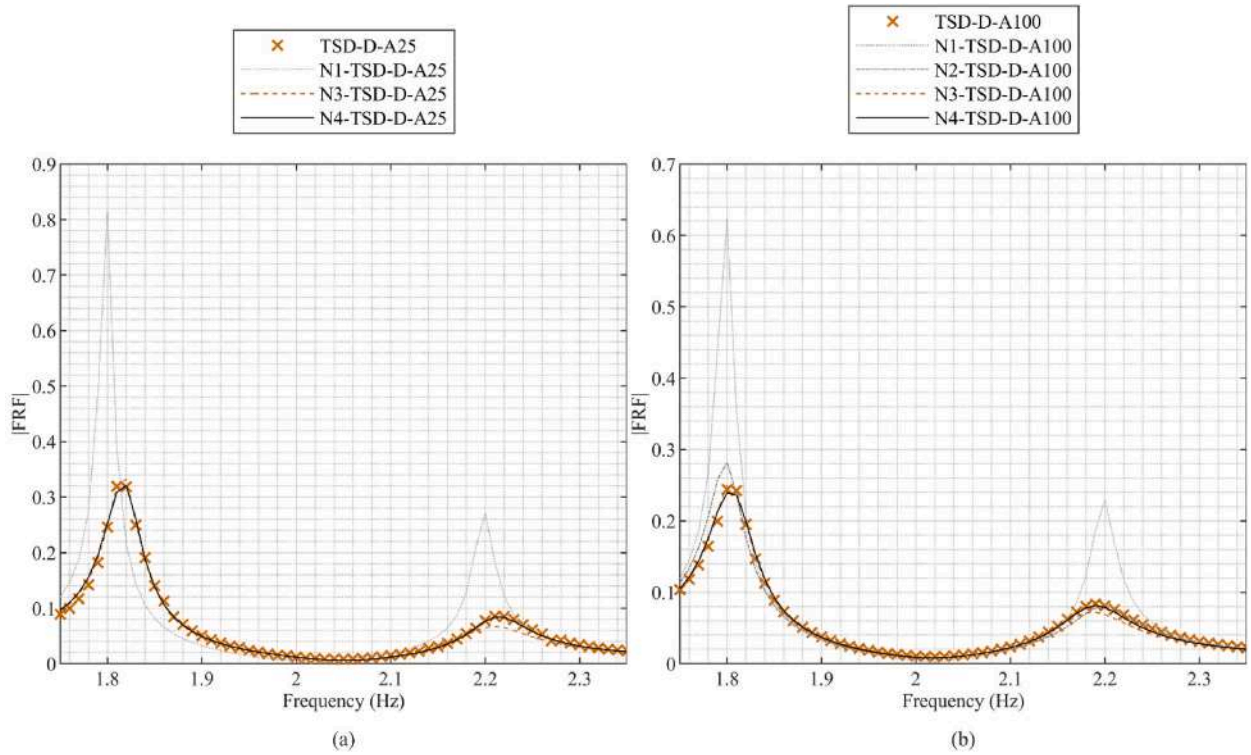

Fig. 36. Experimental and numerical FRF in acceleration of the 4th floor of frame equipped with TSD-D, (a) Amplitude 25 %, (b) Amplitude 100 %.

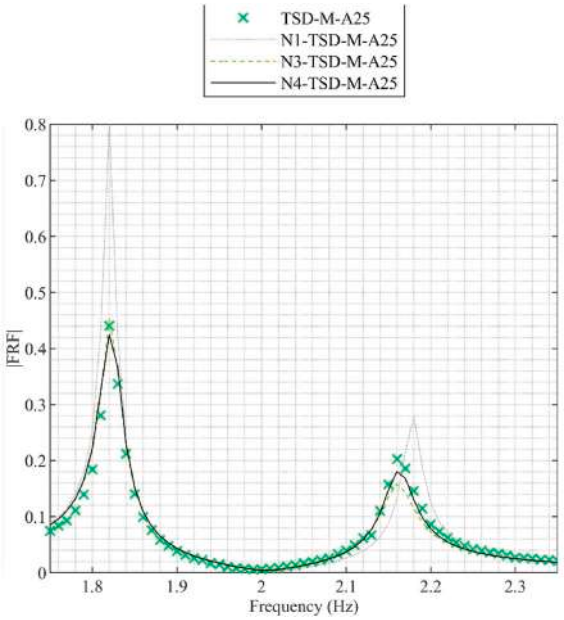

Fig. 37. Experimental and numerical FRF in acceleration of the 4th floor of frame equipped with TSD-M-A25.

tuning is detected, while doubling the damping coefficient provided by N1 is required to meet the optimization results. These show the greatest match for the amplitude-dependent damping ratio form case N4, which takes values of 1.28 % and 0.96 % for the first and second peaks respectively. Once again, the optimization carried out for both N3 and N4 analyses retrieves an effective mass 5 % smaller than expected.

6.3. Fame response equipped with LCVAs

The numerical analysis results of LCVAs for the four cases considered is presented in this section. A summary of the data related to frequency of sloshing (f_1), effective mass (m_1) and damping coefficient of the fluid (ξ) used for the modelling for all the simulations studied crossed with the numerical scenarios is presented in Table 17, along with the value obtained from the minimization of the cost function (C_{FRF}). It is clear that the minimization of the cost function reaches its minimum for the N4 approach, which suggests that the greatest accuracy can be obtained considering slight mistuning, an effective mass of about 20 % of the total fluid mass and fluid damping as a linear dependence of the amplitude of the acceleration variable.

The comparison of the experimental and numerical analyses of the application of LCVA-W on the studied frame can be seen in Fig. 38. Fig. 38a emphasizes that, in this case, following the recommendations proposed in N1 and N2 would lead to imprecise response predictions, when compared to the experimental results. To start with, it is clear from N1 that only a fraction of the total mass

Table 17
LCVA numerical analysis data.

Test name		LCVA-W-A25	LCVA-D-A25	LCVA-M-A25	LCVA-W-A100	LCVA-D-A100
N1	f_1	2.00 Hz	2.00 Hz	2.00 Hz	2.00 Hz	2.00 Hz
	m_1	4.04 kg	4.42 kg	3.52 kg	4.04 kg	4.42 kg
	ξ	0.50 %	0.50 %	0.50 %	0.50 %	0.50 %
	C_{FRF}	1.2395	1.1945	1.1384	.97337	0.9432
N2	f_1	2.00 Hz	2.00 Hz	2.00 Hz	2.00 Hz	2.00 Hz
	m_1	1.25 kg	1.36 kg	1.09 kg	1.25 kg	1.36 kg
	ξ	0.50 %	0.50 %	0.50 %	0.50 %	0.50 %
	C_{FRF}	0.5232	0.9311	0.9098	0.4437	0.6776
N3	f_1	2.03 Hz	1.96 Hz	1.89 Hz	1.96 Hz	1.94 Hz
	m_1	1.01 kg	1.19 kg	1.06 kg	0.91 kg	0.76 kg
	ξ	2.52 %	11.82 %	4.53 %	4.20 %	8.67 %
	C_{FRF}	0.0034	0.0002	0.0073	0.0014	0.0002
N4	f_1	2.03 Hz	1.96 Hz	1.87 Hz	1.96 Hz	1.94 Hz
	m_1	1.01 kg	1.19 kg	1.32 kg	0.89 kg	0.86 kg
	m (ξ)	0.03359	0.03854	0.00002	0.07903	0.06906
	n (ξ)	0.01642	0.11294	0.05262	0.03487	0.08835
	C_{FRF}	0.0021	0.0002	0.0055	0.0012	0.0004

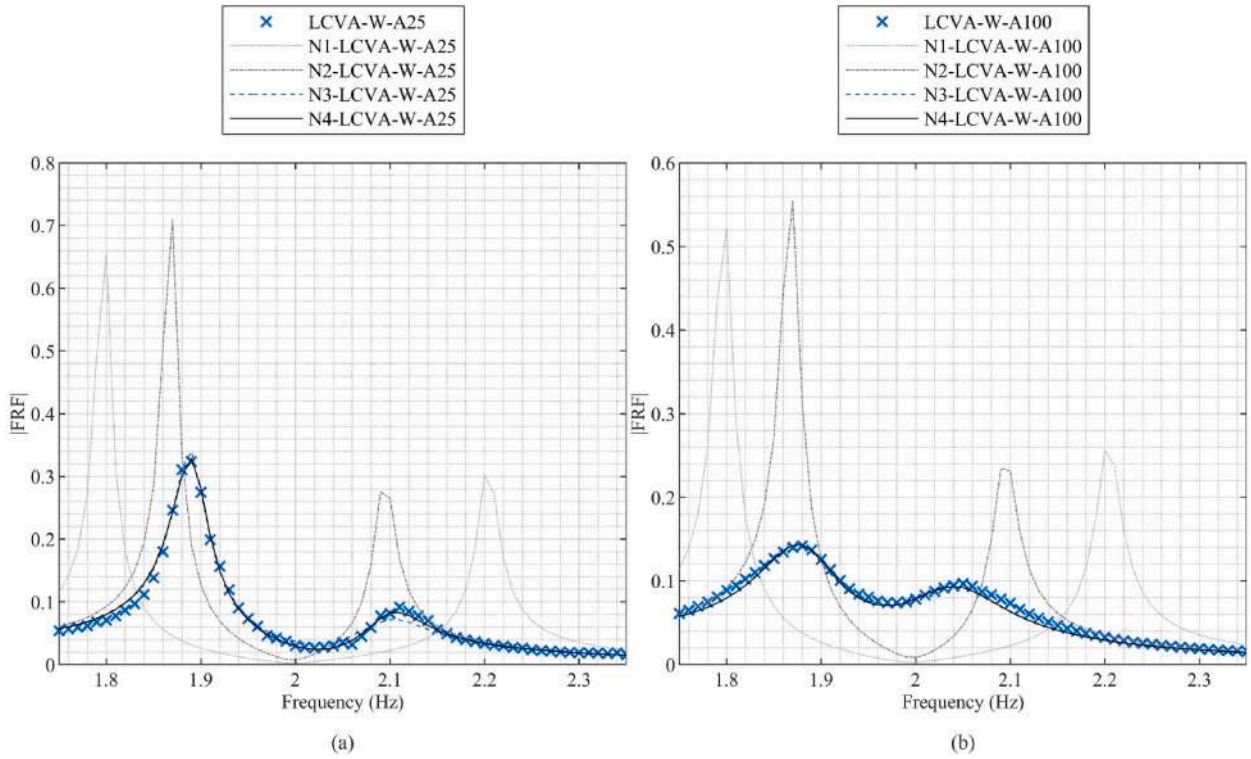

Fig. 38. Experimental and numerical FRF in acceleration of the 4th floor of frame equipped with LCVA-W, (a) Amplitude 25 %, (b) Amplitude 100 %.

participates in the mitigation of vibrations. The results derived from N3 and N4 for the optimised effective mass retrieve values corresponding to 25 % of the total mass, a figure slightly below the mass residing inside the columns which represents 30.84 % of m_{TOT}. Moreover, the model updating retrieves an over-tuning of 1.5 % that shifts the response 0.2 Hz to the right in both N3 and N4 scenarios and suggests that the damping coefficient achieved by LCVA-W-A25 is 5 times higher than that proposed in the literature if considered constant, as in N3, and reaches values of 2.75 % and 1.94 % for the first and second peaks respectively in the linearly variable N4 approach.

By looking at Fig. 38b, similar deductions can be made. In this particular case, the optimised damping coefficient value of LCVA-W-A100 increases up to 4.30 % if considered constant, as in the N3 approach, which can be further refined by using the linearly amplitude dependent damping coefficient reflected in analysis N4, which retrieves 4.59 % and 4.25 % fluid damping for the first and second response peaks. The effective mass can be considered of the same order of magnitude as in the previous case. However, it must be noted that said parameter is smaller when compared to the previously exposed case amplitude A25, representing 22 % of m_{TOT}, which could be attributed to the effect of larger damping partially invalidating mass movement.

The use of the most viscous fluid on LCVAs can be seen in Fig. 39 for A25 and A100 cases. It is shown that the increment in the viscosity leads, together with the type of container, to high values of damping coefficient. Following the N3 constant damping approach, its value is around 12 times bigger than that proposed in the literature in the case of LCVA-D-A25 ($\xi = 11.82$ %) and about 17 ($\xi = 8.67$ %) times in the case of LCVA-D-A100. If considered linearly variable, as in scenario N4, the value obtained at the peak is 11.90 % for the case amplitude A25 and 10.00 % for A100. Regarding the frequency tuning, optimizations N3 and N4 show that in both amplitude cases the frequency achieved by the LCVA was 2 % smaller than the simulated value. As for the effective mass, a behaviour similar to that of LCVA-W is obtained: the effective mass derived from the optimisations N3 and N4 aligns in order of magnitude with the mass of fluid inside the columns, although in both cases it has been found to be slightly smaller. The percentage that participates in the mitigation of vibrations is smaller for large amplitude values from A100, representing 17.2 % and 19.5 % of the total fluid for analysis N3 and N4, while the smaller amplitude tests A25 result in 26.9 % for both N3 and N4 approaches.

The results obtained from the use of the medium-viscosity fluids in LCVAs can be seen in Fig. 40. In this case, an under-tuning is detected to meet the experimental analysis, resulting in 5.4 % and 6.4 % for N3 and N4 approaches respectively. As for the effective mass, the best fit with the experimental results is obtained considering 37.6 % of the total mass, a value that does not align with the previously studied cases LCVA-W and LCVA-D. The influence of fluid viscosity on this kind of containers is manifested: damping ratios of 4.5 % and 5.3 % are obtained for optimizations N3 and at the peak on N4, respectively.

How the inclusion of a perforated screen in the middle horizontal section of LCVAs affects the numerical definition of LCVAs is detailed below. The numerical analysis results of LCVAs for the four cases considered is presented in this section, and Table 18 provides

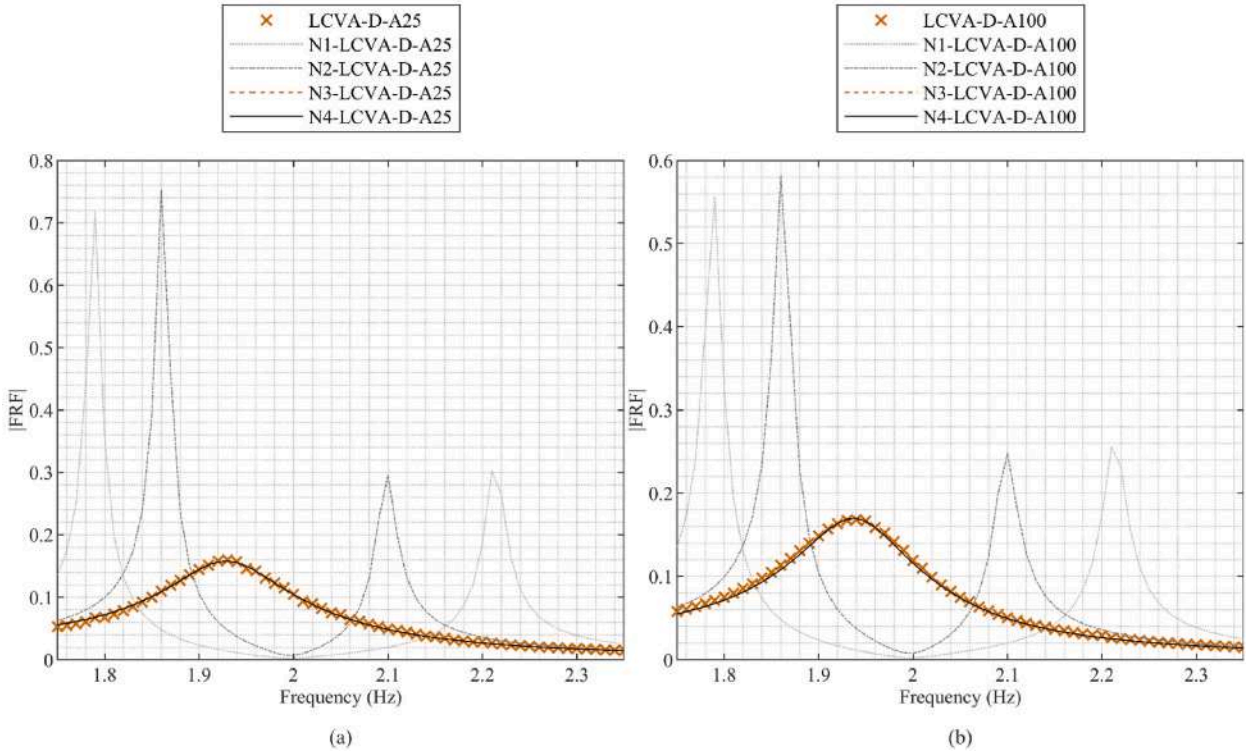

Fig. 39. Experimental and numerical FRF in acceleration of the 4th floor of frame equipped with LCVA-W, (a) Amplitude 25 %, (b) Amplitude 100 %.

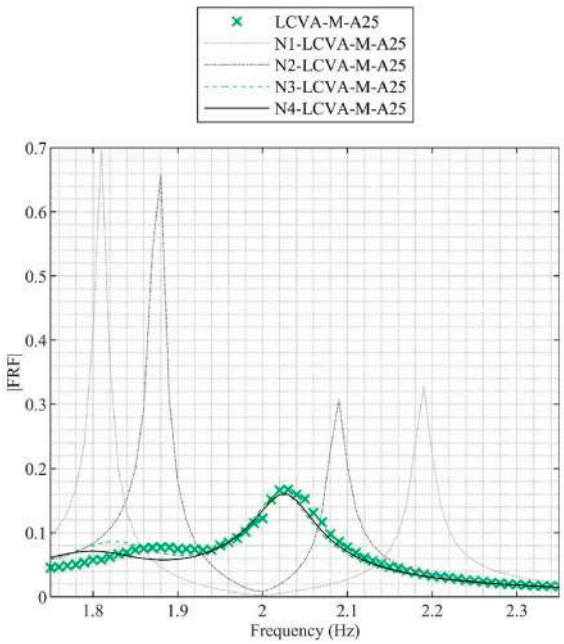

Fig. 40. Experimental and numerical FRF in acceleration of the 4th floor of frame equipped with LCVA-M-A25.

an overview of the data related to the sloshing frequency (f_1), effective mass (m_1), and fluid damping coefficient (ξ) used in the numerical analyses, along with the values obtained from minimizing the cost function (C_{FRF}) for all numerical scenarios.

The FRF outcome of LCVA6-W is plotted in Fig. 41. The numerical results concur with the previously stated observations regarding

Table 18
LCVA6 and LCVA7 numerical analysis data.

Test name		LCVA6-W-A25	LCVA6-W-A100	LCVA7-W-A25	LCVA7-W-A100
N1	f_1	2.00 Hz	2.00 Hz	2.00 Hz	2.00 Hz
	m_1	4.04 kg	4.04 kg	4.04 kg	4.04 kg
	ξ	0.50 %	0.50 %	0.50 %	0.50 %
	C_{FRF}	1.4192	0.9510	1.3422	0.9170
N2	f_1	2.00 Hz	2.00 Hz	2.00 Hz	2.00 Hz
	m_1	1.25 kg	1.25 kg	1.25 kg	1.25 kg
	ξ	0.50 %	0.50 %	0.50 %	0.50 %
	C_{FRF}	1.0369	0.7274	1.1123	0.7115
N3	f_1	2.07 Hz	1.92 Hz	2.08 Hz	1.91 Hz
	m_1	0.84 kg	0.76 kg	0.96 kg	0.83 kg
	ξ	4.38 %	8.54 %	7.10 %	7.56 %
	C_{FRF}	0.0427	0.0025	0.0390	0.0041
N4	f_1	2.07 Hz	1.91 Hz	2.05 Hz	1.90 Hz
	m_1	0.77 kg	0.82 kg	1.47 kg	0.93 kg
	m (ξ)	0.31279	0.31047	0.87852	0.54598
	n (ξ)	0.00559	0.04235	0.01732	0.01123
	C_{FRF}	0.0035	0.0014	0.0137	0.0027

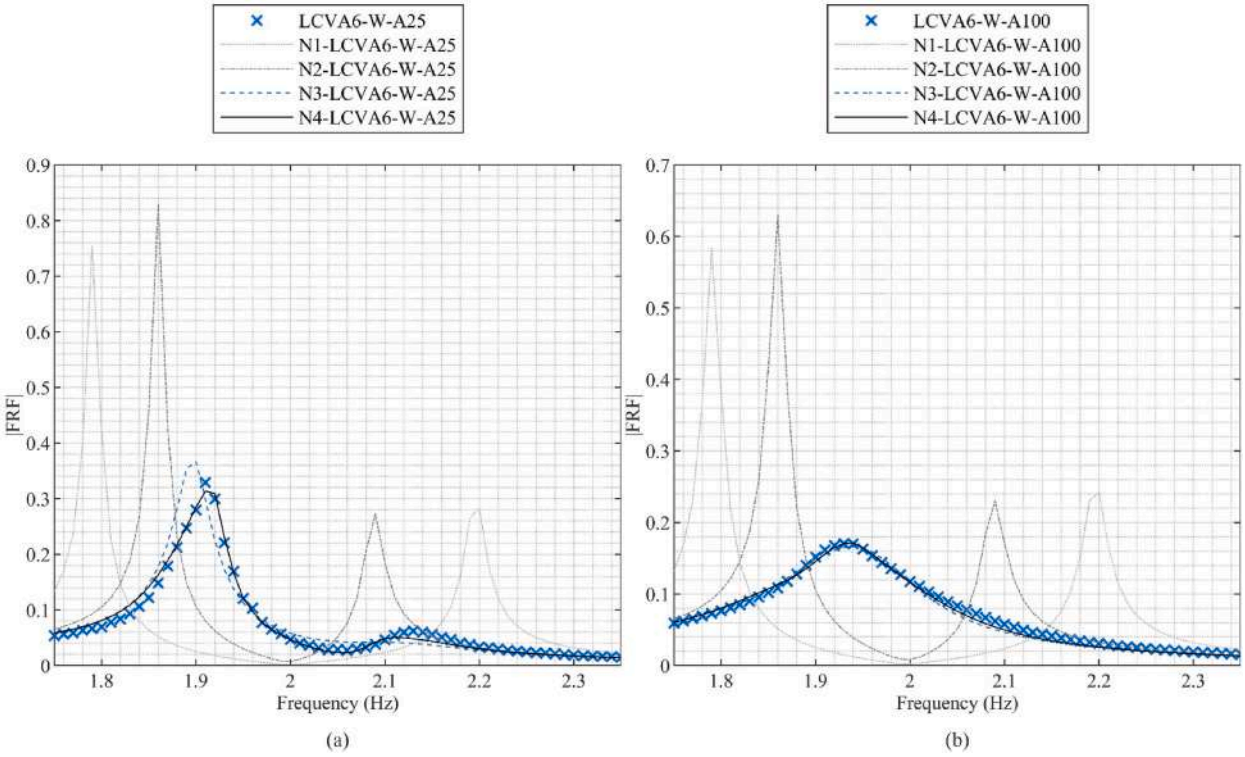

Fig. 41. Experimental and numerical FRF in acceleration of the 4th floor of frame equipped with LCVA6-W, (a) Amplitude 25 %, (b) Amplitude 100 %.

the effective mass of LCVAs: both LCVA6-W-A25 and LCVA6-W-A100 cases retrieve a more accurate solution if the effective mass considered is about 20 % of m_{TOT}, as evidenced from analyses N3 and N4. Focusing on the frequency tuning, it is clear from Fig. 41a that better precision is obtained when the numerical LCVA frequency is over-tuned to 2.07 Hz which could have been derived from millimetrically infra-filling the tanks.

By contrast, Fig. 41b reveals that the frequency value that minimizes the cost function in both N3 and N4 study cases is 1.92 Hz, which instead could have been caused by a millimetric over-filling of the containers. Regarding the fluid damping, considering either constant or linearly variable damping, from N3 and N4 criteria, retrieve more accurate values of a higher and different order of magnitude when compared to the basis of N1 or N2. The greatest precision is obtained when variable damping with the amplitude is considered. Particularly, N4-LCVA6-W-A25 exemplifies the difference in damping for different motions of amplitude, since the first peak, which corresponds to the largest displacement, is obtained for 10.6 % damping ratio, while the second peak is adjusted with $\xi =$

2.50 %. The damping coefficient obtained for the largest amplitude A100 is similar to the one retrieved from A25.

Fig. 42 represents these results for the LCVA7 cases. Regarding the frequency of the device, similar patterns to LCVA6 are obtained: slight over and under tuning for the A25 and A100 cases respectively. Similarly, the effective mass is around 20 % of the total fluid mass. As for the numerical damping ratio, LCVA7-W-A100 shows slightly smaller damping coefficients than LCVA6-W-A100, since the blocked area was smaller. It must be noted that, as an exception, N4-LCVA7-W-A25 optimization results do not align with the trend observed in this work for all remaining LCVAs, since the mass involved in the fluid motion is set to 36.6 % of m_{TOT}, and the resulting damping ratio is 24.57 % for the first peak, values which almost double the expected results.

7. Conclusions

The present study investigates the horizontal vibration control of a multi degree of freedom frame equipped with TLDs through an experimental campaign supported by a comprehensive literature review on the numerical definition of these absorbers. A numerical analysis has been subsequently developed to interpret the experimentally obtained results and to address critical inconsistencies found in existing formulations. In particular, this work clarifies the influence of three key parameters -mass, damping and frequency of the TLD-on their design and performance, proposing new formulations that improve the prediction accuracy and practical applicability of these devices.

The experimental tests and the numerical models compare the efficacy of water and two other commercially available fluids with different viscosities and densities in mitigating the frame response subjected to harmonic base excitation of varying amplitudes using a shaking table. The two main TLD geometrical configurations, that is, TSDs and LCVAs, are considered highlighting how the fluid selection influences their performance. The main findings are:

Regarding TSDs.

- The structural response in terms of roof acceleration was significantly reduced around the resonant frequency for all the fluids considered (by over 99 %).
- The overall maximum response control is directly affected by the fluid viscosity: high viscosity fluid (D) reduced the maximum peak by 84 %, compared to 77 % for medium viscosity fluid (M) and a 68 % reduction achieved by water (W).
- The increment of viscosity leads to greater control of the free surface fluid motion since it supresses sloshing, meaning that, in this particular case, the most viscous fluid was the most suitable choice because it ensured a linear behaviour.

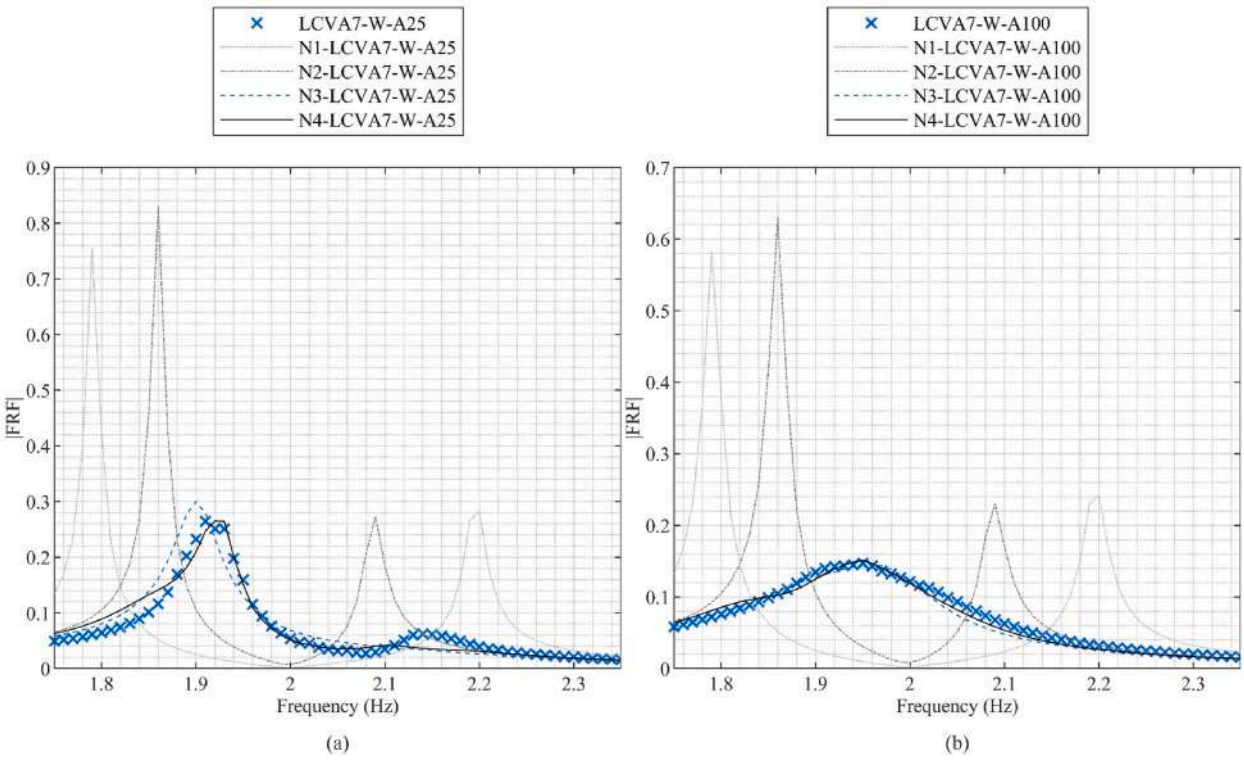

Fig. 42. Experimental and numerical FRF in acceleration of the 4th floor of frame equipped with LCVA7-W, (a) Amplitude 25 %, (b) Amplitude 100 %.

- Numerical analyses confirmed the great accuracy of literature models for the prediction of the percentage of the fluid that participates in the sloshing.
- The greatest inaccuracies derived from the definition of the damping of the fluid. It was clear that the general guidelines for water and other fluids provided by the Eurocodes are conservative.
- Although the best matching results are obtained if the damping of the device is considered to vary linearly with the amplitude of motion, great accuracy can be obtained if constant damping is assumed.
- The constant damping ratio values obtained are similar for all the amplitudes considered:
  - o Fluid W, $\xi \sim 0.5$ %.
  - o Fluid D, $\xi \sim 2.4$ %.
  - o Fluid M, $\xi \sim 1.2$ %.

Regarding LCVAs.

- Response reduction is clear, which was diminished by over 88 % around resonance, but the performance depends clearly on the fluid viscosity.
- Fluids more viscous than water showed a non-optimum response due to an excess in the damping of the device, represented by a single peaked curve response. Similarly, if a perforated screen is added in the middle of the horizontal section an excess in damping can result even when using water as the working fluid.
- For the LCVA proportions considered in this study, water was the most suitable choice.
- The assumption generally found in the literature in which the total fluid mass participates in the vibration mitigation is seen as inaccurate. The findings obtained from this work for the LCVA geometry considered suggest a new effective mass definition, which corresponds to the fraction of the fluid residing inside the columns.
- A novel natural frequency definition is proposed in this paper to accurately define this fundamental parameter. As a result, the prediction error is reduced from 15 % to below 2 %.
- The damping of the LCVAs was also influenced by the amplitude of motion and the fluid viscosity, together with the inclusion of perforated barriers, and the resulting optimised values are greater than those suggested by the literature, which are seen to be on the safe side.
- The constant damping ratio values obtained are greatly influenced by the amplitude of motion:
  - o Fluid W, $\xi \sim 2.5$–4.2 %.
  - o Fluid D, $\xi \sim 8.8$–11.8 %.
  - o Fluid M, $\xi \sim 4.5$ %.

This work presents a thorough study that compares the most commonly used TLD geometrical versions considering the influence of different commercially available non-organic fluids for various input amplitudes on a MDOF scaled frame. The numerical analysis refines the definition of critical parameters -effective mass, damping and natural frequency of the device-addressing inconsistencies found in the literature and proposing improved formulations which might be useful for revising design guidelines. These findings are aimed at enhancing the practical application of TLDs and improving their modelling for their successful implementation on structural vibration control.

CRediT authorship contribution statement

Andrea Vázquez-Greciano: Writing – review & editing, Writing – original draft, Software, Methodology, Investigation, Formal analysis, Conceptualization. **Nicola Buratti:** Supervision, Software, Resources, Methodology, Conceptualization. **Antonio Aznar López:** Visualization, Supervision, Methodology, Conceptualization. **Jesús María Ortiz Herrera:** Visualization, Supervision, Methodology, Conceptualization.

Funding sources

This research did not receive any specific grant from funding agencies in the public, commercial, or not-for-profit sectors.

Declaration of competing interest

The authors declare that they have no known competing financial interests or personal relationships that could have appeared to influence the work reported in this paper.

Acknowledgements

Andrea Vazquez-Greciano would like to acknowledge the support provided by the predoctoral contract Ayuda Programa Propio from the Universidad Politécnica de Madrid.

Data availability

Data will be made available on request.

References

[1] V.J. Modi, F. Welt, Damping of wind induced oscillations through liquid sloshing, J. Wind Eng. Ind. Aerod. 30 (1988) 85–94.
[2] H.F. Bauer, Oscillations of Immiscible Liquids in a Rectangular Container: a New Damper for Excited Structures, 1984.
[3] A. Vázquez-Greciano, A. Aznar López, N. Buratti, J.M. Ortiz Herrera, Magnetic Fields to Enhance Tuned Liquid Damper Performance for Vibration Control: a Review, Springer Science and Business Media B.V, Jan. 01, 2024, https://doi.org/10.1007/s11831-023-09971-4.
[4] T. Konar, A. Ghosh, A Review on Various Configurations of the Passive Tuned Liquid Damper, SAGE Publications Inc, 2022, https://doi.org/10.1177/10775463221074077.
[5] H. ding Sun, H. xiang He, Y. Cheng, Q. Cao, Theoretical and experimental research on vibration control of the tuned liquid damper with damping net and sloped-bottom, J. Build. Eng. 81 (Jan) (2024), https://doi.org/10.1016/j.jobe.2023.108170.
[6] M.B. Navdar, E. Çelebi, T. Engin, H. Dal, F.C. Yılmaz, Experimental and numerical study on vibration mitigation of slender structures with TLCD under second-order effects, J. Build. Eng. 102 (May 2025), https://doi.org/10.1016/j.jobe.2024.111675.
[7] B. Mehrkian, O. Altay, Omnidirectional liquid column vibration absorbers for multi-story buildings, J. Build. Eng. 62 (Dec. 2022), https://doi.org/10.1016/j.jobe.2022.105306.
[8] Y. Fujino, B.M. Pacheco, P. Chaiseri, L.M. Sun, Parametric studies on tuned liquid damper (TLD) using circular containers by free-oscillation experiments, Structural Engineering/Earthquake Engineering 5 (2) (1988) 381–391.
[9] T.G. Lepelletier, F. Raichlen, Nonlinear oscillations in rectangular tanks, J. Eng. Mech. 114 (1) (1988) 1–23.
[10] L.M. Sun, Y. Fujino, B.M. Pacheco, M. Isobe, Nonlinear waves and dynamic pressures in rectangular tuned liquid damper (TLD) - simulation and experimental verification, Struct. Eng. Earthq. Eng. 6 (1989) 81–92.
[11] Y. Fujino, L. Sun, B.M. Pacheco, P. Chaiseri, Tuned liquid damper (TLD) for suppressing horizontal motion of structures, J. Eng. Mech. 118 (10) (1992) 2017–2030.
[12] L.M. Sun, Y. Fujino, P. Chaiseri, B.M. Pacheco, The properties of tuned liquid dampers using a TMD analogy, Earthq. Eng. Struct. Dynam. 24 (1995) 967–976.
[13] D. Reed, J. Yu, H. Yeh, S. Gardarsson, Investigation of tuned liquid dampers under large amplitude excitation, J. Eng. Mech. 124 (4) (1998) 405–413.
[14] L.M. Sun, B.M. Pacheco, Y. Fujino, P. Chaiseri, Effects of liquid viscosity on TLD performance-experiment and simulation, in: Proceedings of, Japan Society of Civil Engineers, 1989, pp. 732–733.
[15] L. Sun, T. Kikuchi, Y. Goto, M. Hayashi, Tuned liquid damper (TLD) using heavy mud, Transactions on the Built Environment 35 (1998) 87–96 [Online]. Available: www.witpress.com.
[16] A. Vázquez-Greciano, C. De Santos-Berbel, A. Aznar López, J.M. Ortiz Herrera, Evaluation of the fluid properties modification through magnetic fields for their application on tuned liquid dampers: an experimental approach, Applied Sciences (Switzerland) 15 (8) (Apr. 2025), https://doi.org/10.3390/app15084194.
[17] S. Das, S. Choudhury, Seismic response control by tuned liquid dampers for low-rise RC frame buildings, Aust. J. Struct. Eng. 18 (2) (Apr. 2017) 135–145, https://doi.org/10.1080/13287982.2017.1351180.
[18] A. Ocak, G. Bekdaş, S.M. Nigdeli, S. Kim, Z.W. Geem, Optimization of tuned liquid damper including different liquids for lateral displacement control of single and multi-story structures, Buildings 12 (3) (Mar. 2022) 377, https://doi.org/10.3390/buildings12030377.
[19] Y. Xin, G. Chen, M. Lou, Seismic response control with density-variable tuned liquid dampers, Earthq. Eng. Eng. Vib. 8 (4) (Dec. 2009) 537–546, https://doi.org/10.1007/s11803-009-9111-7.
[20] F. Sakai, S. Takeda, T. Tamaki, Tuned liquid column damper-new type device for suppression of building vibration, in: Proceedings of the International Conference on High Rise Buildings, 1989, pp. 926–931. Nanjing.
[21] B. Samali, K.C.S. Kwok, D. Tapner, Vibration control of structures by tuned liquid column dampers, in: IABSE Congress Report = Rapport Du Congrès AIPC = IVBH Kongressbericht, 1992, pp. 461–466, https://doi.org/10.5169/seals-13862.
[22] T. Balendra, C.M. Wang, H.F. Cheong, Effectiveness of tuned liquid column dampers for vibration control of towers, Eng. Struct. 17 (9) (1995) 66–675.
[23] H. Gao, K.C.S. Kwok, B. Samali, Optimization of tuned liquid column dampers, Eng. Struct. 19 (6) (1997) 476–486.
[24] Y.L. Xu, B. Samali, K.C.S. Kwok, Control of along-wind response of structures by mass and liquid dampers, J. Eng. Mech. 118 (1) (1992) 20–39.
[25] A.Y.J. Won, J.A. Pires, M.A. Haroun, Performance assessment of tuned liquid column dampers under random seismic loading, Int J Non Linear Mech 32 (4) (1997) 745–758.
[26] P.A. Hitchcock, K.C.S. Kwok, R.D. Watkins, B. Samali, Characteristics of liquid column vibration absorbers (LCVA)-II, Eng. Struct. 19 (2) (1997) 135–144.
[27] P.A. Hitchcock, K.C.S. Kwok, R.D. Watkins, B. Samali, Characteristics of liquid column vibration absorbers (LCVA) I, Eng. Struct. 19 (2) (1997) 126–134.
[28] C.C. Chang, C.T. Hsu, Control performance of liquid column vibration absorbers, Eng. Struct. 20 (7) (1998) 580–586.
[29] C.C. Chang, Designing water dampers for suppressing along-wind and cross-wind building vibration, Hong Kong Institution of Engineers Transactions 5 (3) (1998) 17–24.
[30] J.-H. Park, K.-W. Min, Optimal shape of LCVA for vibration control of structures subjected to along wind excitation, Smart Struct. Syst. 10 (6) (2012) 573–591.
[31] M.F. Younes, Effect of different design parameters on damping capacity of liquid column vibration absorber, J. Eng. Appl. Sci. 65 (6) (2018) 447–467 [Online]. Available: https://www.researchgate.net/publication/329732488.
[32] S. Saha, R. Debbarma, Dynamic response control of structures using liquid column vibration absorber: an experimental study, International Journal of Advanced Structural Engineering 9 (3) (Sep. 2017) 269–275, https://doi.org/10.1007/s40091-017-0163-z.
[33] L. Son, Marshal, M. Bur, Empirical evaluation of variation of orifice blocking ratio in a tuned liquid column damper using frequency response function measurement, Int. J. Adv. Sci. Eng. Inf. Technol. 8 (2) (2018) 489–494, https://doi.org/10.18517/ijaseit.8.2.4163.
[34] M.M. Abou Elenin, Y.K. Younes, M.F. Younes, An experimental study on the damping characteristics and tuning of the liquid column vibration absorber, J Phys Conf Ser 2299 (1) (2022), https://doi.org/10.1088/1742-6596/2299/1/012007.
[35] S. Colwell, B. Basu, Experimental and theoretical investigations of equivalent viscous damping of structures with TLCD for different fluids, J. Struct. Eng. 134 (2008) 154–163, https://doi.org/10.1061/ASCE0733-94452008134:1154.
[36] L. Son, M. Bur, M. Rusli, Evaluation of TLCD damping factor from FRF measurement due to variation of the fluid viscosity, KnE Engineering 2016 (1) (Sep. 2016), https://doi.org/10.18502/keg.v1i1.481.
[37] M. Reiterer, A. Kluibenschedl, LIQUID DAMPER FOR REDUCING VERTICAL AND/OR HORIZONTAL VIBRATIONS IN A BUILDING OR MACHINE STRUCTURE, 2010.
[38] M. Tanveer, M. Usman, I.U. Khan, S.H. Farooq, A. Hanif, Material optimization of tuned liquid column ball damper (TLCBD) for the vibration control of multi-storey structure using various liquid and ball densities, J. Build. Eng. 32 (Nov. 2020), https://doi.org/10.1016/j.jobe.2020.101742.
[39] M. Péntek, A. Riedl, K.U. Bletzinger, F. Weber, Investigating the vibration mitigation efficiency of tuned sloshing dampers using a two-fluid CFD approach, Applied Sciences (Switzerland) 12 (14) (Jul. 2022), https://doi.org/10.3390/app12147033.
[40] D. Han, X. Li, W. Wang, X. Su, Vibration suppression performance comparison of floating offshore wind turbines using a tuned liquid column damper and a tuned mass damper, Ocean Engineering 330 (Jun. 2025), https://doi.org/10.1016/j.oceaneng.2025.121285.
[41] Y.E. Kebeli, E. Aydın, B. Öztürk, H. Çetin, Experimental comparison of the performance of shear frame with TLD and TLCD under harmonic ground motion, Buildings 14 (12) (Dec. 2024), https://doi.org/10.3390/buildings14123843.
[42] E. Aydin, B. Öztürk, M. Bati, Y. Kavaz, B. Kilinc, Effects of tuned liquid column damper properties on the dynamic response of structures, in: EMI International Conference, 2019, p. 198. Lyon, France.

[43] E. Aydin, B. Öztürk, H. Çetin, M. Dutkiewicz, O. Okkay, U. Ohancan, Experiments of tuned liquid column damper (TLCD) on the reduced shear frames under harmonic loads, in: 16th European Conference on Earthquake Engineering (16ECEE), 2018. Thessaloniki, Greece.
[44] E. Aydln, et al., Experiments of tuned liquid damper (TLD) on the reduced shear frame model under harmonic loads, in: EPJ Web of Conferences, EDP Sciences, May 2017, https://doi.org/10.1051/epjconf/201714302001.
[45] H. Frahm, DEVICE FOR DAMPING VIBRATIONS OF BODIES, Oct. 30, 1909 989958.
[46] B. Weber, G. Feltrin, Assessment of long-term behavior of tuned mass dampers by system identification, Eng. Struct. 32 (11) (Nov. 2010) 3670–3682, https://doi.org/10.1016/j.engstruct.2010.08.011.
[47] F. Tubino, G. Piccardo, Tuned mass damper optimization for the mitigation of human-induced vibrations of pedestrian bridges, Meccanica 50 (3) (Jan. 2015) 809–824, https://doi.org/10.1007/s11012-014-0021-z.
[48] D. Wang, T.K.T. Tse, Y. Zhou, Q. Li, Structural performance and cost analysis of wind-induced vibration control schemes for a real super-tall building, Struct. Infrastruct. Eng. Maint., Manag. Life-Cycle Des. Perform. 11 (8) (Aug. 2014) 990–1011, https://doi.org/10.1080/15732479.2014.925941.
[49] F. Sadek, B. Mohraz, A.W. Taylor, R.M. Chung, A method of estimating the parameters of tuned mass dampers for seismic applications, Earthq. Eng. Struct. Dynam. 26 (1997) 617–635.
[50] G.W. Housner, Dynamic pressures on accelerated fluid containers, Bull. Seismol. Soc. Am. 47 (1) (1957) 15–35.
[51] G. Michele Calvi, Roberto Nascimbene, Progettazione sismica dei serbatoi, in: Progettare i Gusci. Acciaio, Cemento Armato E Precompresso. Piastre, Serbatoi, Cupole, Paraboloidi E Condotte. Gravità, Instabilità E Azioni Sismiche, IUSS Press, 2011, pp. 537–672.
[52] M.J.N. Priestley, J.H. Wood, B.J. Davidson, SEISMIC DESIGN OF STORAGE TANKS, vol. 4, Bulletin of the New Zealand National Society for Earthquake Engineering, 1986, pp. 272–284.
[53] ACI 350.3-06, Seismic Design of Liquid -Containing Concrete Structures and Commentary, 2006.
[54] P. Malhotra, Practical nonlinear seismic analysis of tanks, Earthq. Spectra 16 (2) (2000) 473–492, https://doi.org/10.1193/1.1586122.
[55] G.W. Housner, The dynamic behaviour of water tanks, Bull. Seismol. Soc. Am. 53 (2) (1963) 381–387.
[56] J.-K. Yu, T. Wakahara, D.A. Reed, A non-linear numerical model of the tuned liquid damper, Earthq. Eng. Struct. Dynam. 28 (1999) 671–686.
[57] M.E. Accioly, L.P.C. Melo, T.D. de Araújo, Analytical evaluation of water supply tanks as dampers, in: *Proceedings of the XXXVIII Iberian Latin American Congress on Computational Methods in Engineering*, ABMEC Brazilian Association of Computational Methods in Engineering, 2017, https://doi.org/10.20906/cps/cilamce2017-0789.
[58] L. Sun, Semi-Analytical Modelling of Tuned Liquid Damper (TLD) with Emphasis on Damping of Liquid Sloshing, University of Tokyo, 1991.
[59] L.M. Sun, Y. Fujino, B.M. Pacheco, P. Chaiseri, Modelling of tuned liquid damper (TLD), Journal of Wind Engineering and lndustrial Aerodynamics 41–44 (1992) 1883–1894.
[60] M.J. Tait, Modelling and preliminary design of a structure-TLD system, Eng. Struct. 30 (10) (Oct. 2008) 2644–2655, https://doi.org/10.1016/j.engstruct.2008.02.017.
[61] UNE ENV 1998-4. Eurocode 8: design of structures for earthquake resistance. Part 4: Silos, tanks and pipelines.".
[62] J.C. Wu, M.H. Shih, Y.Y. Lin, Y.C. Shen, Design guidelines for tuned liquid column damper for structures responding to wind, Eng. Struct. 27 (13) (Nov. 2005) 1893–1905, https://doi.org/10.1016/j.engstruct.2005.05.009.
[63] P. Chaiviriyawong, P. Panedpojaman, S. Limkatanyu, T. Pinkeaw, Simulation of control characteristics of liquid column vibration absorber using a quasi-elliptic flow path estimation method, Eng. Struct. 177 (Dec. 2018) 785–794, https://doi.org/10.1016/j.engstruct.2018.09.088.
[64] P. Chaiviriyawong, S. Limkatanyu, T. Pinkaew, Simulations of characteristics of tuned liquid column damper using an elliptical flow path estimation method, in: The 14th World Conference on Earthquake Engineering, 2008. Beijing, China.
[65] M.U. Shah, M. Usman, S.H. Farooq, I.H. Kim, Effect of tuned spring on vibration control performance of modified liquid column ball damper, Applied Sciences 12 (1) (Jan. 2022) 103390, https://doi.org/10.3390/app12010318.
[66] S.M. Zahrai, S. Abbasi, B. Samali, Z. Vrcelj, Experimental investigation of utilizing TLD with baffles in a scaled Down 5-story benchmark building, J Fluids Struct 28 (Jan. 2012) 194–210, https://doi.org/10.1016/j.jfluidstructs.2011.08.016.
[67] Q. Xie, D. Xu, Y. Zhang, Y. Yu, W. Hao, Shaking table testing and numerical simulation of the seismic response of a typical China ancient masonry tower, Bull. Earthq. Eng. 18 (1) (Jan. 2020) 331–355, https://doi.org/10.1007/s10518-019-00731-z.
[68] A. Romanazzi, D. Scocciolini, M. Savoia, N. Buratti, Iterative hierarchical clustering algorithm for automated operational modal analysis, Autom Constr 156 (Dec. 2023) 105137, https://doi.org/10.1016/j.autcon.2023.105137.
[69] B. Peeters, G. De Roeck, Stochastic system identification for operational modal analysis: a review, Journal of Dynamic Systems, Measurement and Control, Transactions of the ASME 123 (4) (2001) 659–667, https://doi.org/10.1115/1.1410370.
[70] D. Brown, W. Christian, R.M. Hanson, Tracker video analysis and modelling tool [Online]. Available:, Version 6.0.3, 2021. https://physlets.org/tracker/. (Accessed 7 August 2024).
[71] Y. Fujino, L.M. Sun, VIBRATION CONTROL BY MULTIPLE TUNED LIQUID DAMPERS (MTLDs), J. Struct. Eng. 119 (12) (1993) 3482–3502.
[72] A.K. Chopra, DYNAMICS OF STRUCTURES; Theory and Applications to Earthquake Engineering, Fourth., 2012.
[73] UNE EN 1998-1. Eurocode 8: Design of Structures for Earthquake Resistance. Part 1: General Rules, Seismic Actions and Rules for Buildings".